CAPTURE COEFFICIENTS OF CARBON DIOXIDE AND NITROGEN GAS ON A CRYOGENIC COOLED SURFACE

LOUIS CARMELO TEDESCHI

CAPTURE COEFFICIENTS OF CARBON DIOXIDE AND NITROGEN GAS ON A CRYOGENIC COOLED SURFACE

by

Louis Carmelo Tedeschi
Lieutenant, United States Navy
B.S., Massachusetts Institute of Technology, 1960

Submitted in partial fulfillment
for the degree of

MASTER OF SCIENCE IN MECHANICAL ENGINEERING

from the

UNITED STATES NAVAL POSTGRADUATE SCHOOL
May 1966

ABSTRACT

Capture coefficients of CO_2 and N_2 were measured on a flat cryopanel. The cryopumping of 300°K CO_2 on an 85°K surface resulted in a capture coefficient of 0.58 while for 300°K N_2 on a 33°K surface a coefficient of 0.65 was measured.

The pressure drop method employed to measure the above capture coefficients was studied to account for vapor pressure, temperature corrections, and assumptions which must be made in the calculation of the capture coefficient. An analog model of the actual system was capable of predicting system pressure responses.

Instrumentation and construction of gaseous helium transfer lines necessary to effect the above measurements are also discussed.

ACKNOWLEDGEMENTS

The work described herein was made possible by the continued support of the Office of Naval Research through the Foundation Research Program.

The author wishes to express his gratitude to Professor Paul F. Pucci for his continued support and encouragement. He also wishes to thank Messrs. K. Smith and H. Harriman for their many helpful suggestions and assistance, and especially Messrs. J. Beck and K. Mothersell for their generous and enthusiastic assistance in the construction and assembly of the system.

TABLE OF CONTENTS

LIST OF ILLUSTRATIONS

TABLES

LIST OF SYMBOLS

A	surface area	cm^2
A_p	cryosurface area	cm^2
C	capture coefficient	
C_e	conduction coefficient	
C_g	condensation coefficient	
C_s	evaporation coefficient	
C_1	conduction coefficient	
k	Boltzmann's Constant	
M	molecular weight	$erg\text{-}°K^{-1}$
N	total number of molecules	
N_o	Avogardo's Number	$molecules\text{-}mole^{-1}$
$\dot{N}_c$	flow of condensation molecules	$molecules\text{-}sec^{-1}$
$\dot{N}_D$	flow of molecules to diffusion pum	$molecules\text{-}sec^{-1}$
$\dot{N}_g$	flow of molecules outgassing	$molecules\text{-}sec^{-1}$
$\dot{N}_{gl}$	molecular flow from V_g to V_1	$molecules\text{-}sec^{-1}$
$\dot{N}_L$	flow of molecules into V_e from gas addition system	$molecules\text{-}sec^{-1}$
N_{21}	flow of molecules from volume 2 to 1	$molecules\text{-}sec^{-1}$
P	total pressure	torr
P_e	pressure in volume V_e	torr
P_1	pressure in volume V_1	torr
Q	throughput rate	$torr\text{-}liters\text{-}sec^{-1}$
R	universal gas constant	$ergs\ °K^{-1}gm\text{-}mole^{-1}$
S_{th}	theoretical pumping speed	$liters\ sec^{-1}cm^{-2}$

List of Symbols (Cont'd)

T_e	temperature of walls of V_e	°K
T_g	temperature of walls of V_g	°K
T_L	temperature of gas admitted into V_e	°K
V_e	volume of gas injection tubing	liters
V_g	volume inside radiation shielding	liters
V_l	volume between radiation shielding walls	liters
V-L	gas injection stop valve	
V-1	high vacuum valve	
$\dot{V}_D$	diffusion pump volumetric flow rate	liters sec^{-1}
α	diffusion pump efficiency factor	
e	emmissivity	
μ	micron	mm Hg x 10^{-3}
σ	Stefan-Boltzmann constant	watts cm^{-2} $°K^{-4}$

1. Introduction

With the advent of the space age, the simulation of the space environment for pre-flight engineering tests of components and entire systems has become of great practical importance. During the past decade, theproduction of high and ultra high vacuum has evolved from the small laboratory research systems to the enormous enclosures capable of testing entire space vehicles.

The limitations in the achievement of a vacuum of 10^{-7} to 10^{-13} mm of Hg are due to the outgassing nature of the metal and components of the chamber walls and the test object, as well as the inevitable leakage of gases from the atmosphere through walls, seals, and gaskets. It has been found that mechanical means of removing these gases is limited and that the most efficient method is to "freeze" these gas molecules on a cold surface (1). The use of liquified gases such as Helium, Hydrogen, and Nitrogen affords a convenient means of obtaining a sufficiently cold surface to condense most gases, for example, at liquid nitrogen temperature (77°K), the uncondensable gases are O_2, N_2, CO, Ne, H_2 and He. Although gaseous helium refrigerators are initially more expensive, the operating costs and temperatures achieved (10-30°K) make them preferable to the use of the cryogenic liquids.

It is thus desirable to predict the ability of such cryogenic cooled surfaces to capture or freeze condensable gases. The relative measure of this capacity,called the capture coefficient or sticking coefficient, is most commonly defined as the probability that a gas molecule will condense on a cold surface on its first encounter with that surface (2). Data on capture coefficient is not abundant, but a great deal is being

gathered as part of a continuing study by ARO, Inc. in research sponsored by Arnold Engineering Development Center (4,12,20).

In considering factors which affect the capture coefficient, the temperature of the gas and the cryosurface as well as the equilibrium pressure were first studied (2,3). In this study it was also discovered that the condition of the surface and thickness of the cryodeposit were also factors. Another observed phenomena was that of one gas physically trapping another; thus, various combinations of gases have been studied. In a recent report several other parameters such as the molecular weight of the gas, Debye characteristic temperature, heat of condensation, polarization and dipole moment, surface area, and surface energy per unit area were investigated to gain a basic understanding of the gas-solid interface phenomena (4). Future studies in directed flow cryopumping are designed to investigate the nature of the irreversible process a molecule encounters upon collision with a cryosurface (5). It is hoped that a continuing study at the U. S. Naval Postgraduate School can correlate available data and add to the general understanding of capture coefficients.

2. Cryopumping

The impact of cryopumping on the production of high vacuum can best be understood by the limitations imposed by mechanical pumps and oil diffusion pumps which were previously the mainstay of high vacuum production.

The limit on ultimate vacuum in a mechanical pump is set by leakage back through the pump, a rotary seal pump such as that employed in this system usually has a blank-off pressure of about 10^{-4} torr. (1 torr = 1 mm Hg). While there is no theoretical limit for vapor stream pumps such as the diffusion pump employed, the size required for a specific pumping speed must be considered (6). The diffusion pump employed has a diameter of 6 inches and a maximum pumping speed of 1500 liters/sec from 10^{-3} to 10^{-5} torr. Diffusion pumps can be purchased with pumping speeds as great as 95,000 liters/sec from $2x10^{-4}$ to 10^{-9} torr, but one of this capacity is 48 inches in diameter and weighs 3320 lbs. Another consideration is the vapor pressure of the oil employed. Although backstreaming of diffusion pump oil is greatly reduced by cryogenic traps, pumping speed is sacrificed because of the necessary restricting conductance of the trap; furthermore, a trap cannot be entirely effective.

The use of cryogenic panels to condense vapors is most efficient because of the high theoretical pumping speeds. A pumping speed of 11.9 liters/sec-cm^2 can be obtained for Nitrogen gas at 300°K with a 60% efficiency at a cryopanel temperature of 20°K. It can be seen that a surface area of only 13,300 cm^2 (14.3 ft^2) is required to match the pumping speed of the massive 48" diffusion pump and this area is only 20 per cent larger than the cross sectional area of this pump. Of course, the

diffusion pump can pump both condensable and non-condensable vapors while the usefulness of the cryogenic surface is limited eventually by the frost accumulated on the surface and the necessity of warming the panel to evaporate the condensate layer. When used with diffusion pumps, the life of the cryopanel can be greatly enhanced since the diffusion pump first reduces the pressure where the density of vapors is greatly reduced and the time for the condensate layer to build up consequently increased. Another limitation on cryopumping involves the cost of maintaining a surface at a temperature below the boiling point of Helium in order to condense all gases including Hydrogen. Cryosoprtion offers a more economical solution to the removal of Hydrogen gas; present research employing all the above methods of pumping indicates that pressures less than 10^{-13} torr should be achievable (7,8).

3. Condensation Phenomena

The condensation phenomena which characterizes cryopumping is of interest to many scientific fields because it is a solid-gas interface problem that in chemistry, for example, determines the rate of reactions and nature of catalytic action.

The basic problem simply stated is to determine the mechanism by which a gaseous atom interacts with atoms on the surface of a solid upon collision with that solid. There have been many approaches to the problem, from a statistical mechanics treatment of microscopic interactions to a macroscopic approach treating the gases involved as having Maxwell-Boltzmann distributions.

Lennard Jones's work characterizes the statistical mechanics approach in which he derives a theory of evaporation of atoms from a solid surface when an adsorbed atom can vibrate radially and laterally about its point of attachment but cannot migrate (9), and also for an atom which can migrate, but vibrates only in a direction normal to the surface (10).

Buffham, et al. characterize the macroscopic approach in their consideration of the critical velocity and condensation-evaporation models (11).

Yet another approach investigated by Dawson and Haygood proposes a potential well-energy barrier model as shown in Figure 1 (12). The gas atom approaches at an average energy ϵ_1, undergoes some unspecified irreversible energy exchange, and is re-emitted if the remaining energy is greater than the threshold energy ϵ_2, of the atom on the cryosurface. The incorporation of an irreversible process with a potential well or

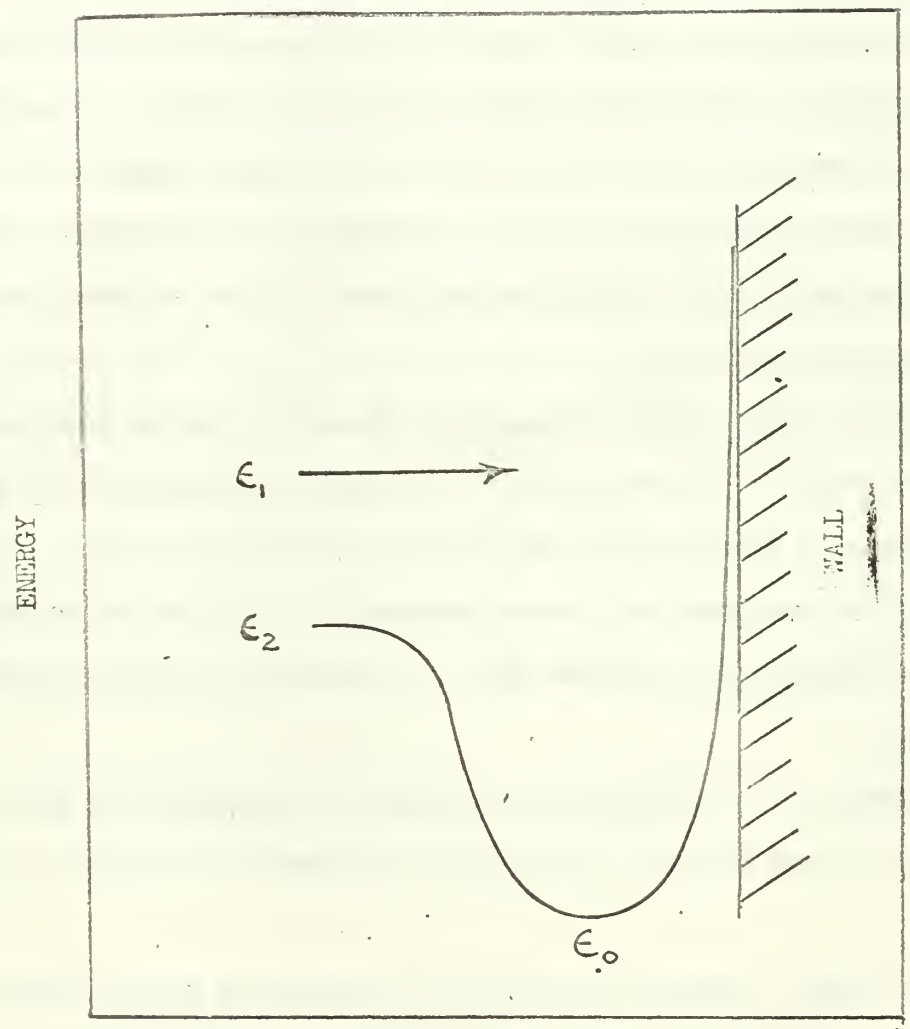

FIG. 1 POTENTIAL WELL MODEL OF CRYOSURFACE

energy barrier concept constitutes a deviation from the classical approach where only reversible processes are considered for these models.

In all the above approaches, the center of interest is the effectiveness of capture, or retainment, by the surface. In each approach a definition for the capture coefficient results.

Lennard-Jones derived an equation for the probability of condensation per collision averaged over all velocities of approach and all states of adsorption. The definition in the macroscopic approach is the ratio of actual number of moles of gas condensed to those theoretically impinging on the cold surface. In microscopic terms this can be thought of as the probability of capture for a molecule on its first encounter with a cold surface.

The latter definition lends itself more readily to physical measurement, for the theoretical pumping speed can be easily calculated from kinetic theory and it therefore remains to measure the actual pumping rate. However, the assumptions that must be made to validate this simplified approach must be closely considered.

4. Measurement of the Capture Coefficient

Considerations in the measurement of the capture coefficient can be classed as follows:

(1) Basic assumptions necessary for the macroscopic approach to be valid.

(2) Factors arising from the experimental technique employed.

Detailed considerations will be peculiar to the system employed, although the approach is general and follows in some ways that of Haygood and Dawson (13).

4.1 Definition of the Capture Coefficient

Consider first the ideal model where a chamber contains only the condensable gas under consideration. When a cold surface is introduced, molecules inpinging on it will be condensed if the pressure of the gas in the chamber is above the vapor pressure corresponding to the condensate temperature. Gas will continue to be condensed until the rate of condensation is equal to the rate of evaporation from the surface.

We can consider the cryopanel to be like an orifice separating two chambers as shown in Fig. 2.

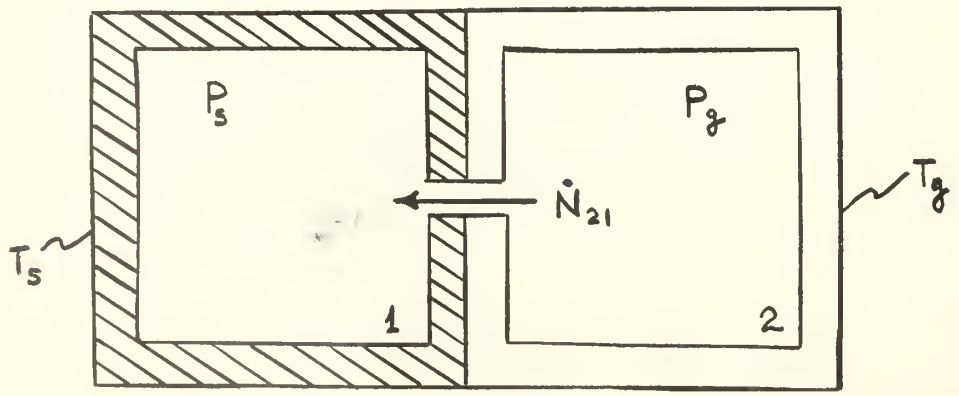

Fig. 2
Model of Cryosurface

One chamber has its wall maintained at temperature T_s, which corresponds to the temperature of the cold surface, and the other wall is maintained at a temperature T_g, corresponding to the temperature of the radiation shielding that encompasses the cryopanel in this system (Fig. 12).

Since we are studying the phenomena of cryopumping in the free molecular flow regime where the mean free path is several times greater than any linear dimensions in the system, intermolecular collisions are rare, and therefore, the temperature of the gas is essentially the temperature of the walls. It must also be assured that the temperature of the wall is uniform, or the Maxwellian distribution, which has been assumed in the macroscopic approach, will be distorted. The result of this distortion is that the temperature of the gas is no longer the temperature of any part of the wall, and further, the gas has no characteristic temperature which can be determined. In this case, a statistical approach using Monte Carlo Methods and a trace of the history of each gas molecule would have to be employed.

It can be shown from an assumption of the above distribution law that the number of molecules striking a surface per unit time is given by

$$\dot{N} = \frac{N}{V} \frac{V_A}{4} A \tag{4.1}$$

where

N = total number of molecules

V = volume

V_A = average molecular velocity

A = surface area

The average velocity also given by the distribution law

$$V_A = \sqrt{\frac{8R_M T}{\pi M}} \tag{4.2}$$

where

R_M = universal gas constant

T = characteristic temperature of the gas

M = molecular weight of the gas

Consider the ideal gas equation of state to hold since the assumption of no intermolecular collisions is nearly the case in the free molecular flow regime. Then, the number of molecules present in a chamber with a given pressure P, volume V, is

$$N = \left(\frac{PV}{R_M T}\right) N_o \tag{4.3}$$

where

N_o = Avogadro's number

T = temperature of the gas

Combining equations (4.1) - (4.3) gives an expression for molecular flux on a surface in terms of measurable quantities.

$$\dot{N} = \frac{PAN_o}{\sqrt{2\pi M R_M T}} \tag{4.4}$$

or

$$\dot{N} = \frac{PA}{\sqrt{2mkT}} \tag{4.5}$$

where $m = \frac{M}{N_o}$ = molecular weight

$k = \frac{R_M}{N_o}$ = Boltzmann's constant

Returning to Figure 2, considering the orifice to be of area A, the net flow of molecules across the orifice into volume 1 is

$$\dot{N}_{21} = \frac{P_g A}{\sqrt{2\pi m k T_g}} - \frac{P_s A}{\sqrt{2\pi m k T_s}} \tag{4.6}$$

where

P_g = the pressure of gas at temperature T_g

P_s = the pressure of gas at temperature T_s

The model described can be considered as an idealization of the condensation phenomena. The rate of condensation is represented by the flux of molecules passing through the orifice from volume 2 to 1, while the rate of evaporation is the flux of molecules from volume 1 to 2. In the free molecular flow regime, each flux is independent of the other, and thus the net rate of condensation is represented by equation (4.6).

The actual rates of evaporation and condensation are less than the molecular fluxes described by (4.5). The ratio of actual to theoretical fluxes are defined by the following coefficients:

C_g = condensation coefficient

C_s = evaporation coefficient

Then, the flow of molecules into volume 1, or captured by the cryopanel are

$$\dot{N}_c = \frac{A_p}{2\pi m k} \left(\frac{C_g P_g}{\sqrt{T_g}} - \frac{C_s P_s}{\sqrt{T_s}} \right) \tag{4.7}$$

where

A_p = cryopanel area

Eventually equilibrium, defined to be no net flow of molecules from one volume to the other, will be established between the two volumes. Under this condition,

$$\frac{C_g P_c}{\sqrt{T_g}} = \frac{C_s P_s}{\sqrt{T_s}} \tag{4.8}$$

When a continuous stream of gas is being injected into Volume 2, steady state will be established as the rate of molecules being admitted into volume 2 equals the net rate of molecules flowing into volume 1. The pressure in volume 2 will be different in steady state with flow being admitted than without influx of gas, the net flow into volume 1 may be represented by

$$\dot{N}_c = \frac{A_p}{\sqrt{2\pi m k}} \left(\frac{C_g P_c}{\sqrt{T_g}} - \frac{C_s P_s}{\sqrt{T_s}} \right) \tag{4.9}$$

where P_c = steady state chamber pressure with flow of gas admitted.

A comparison of (4.9) with (4.7) reveals the same form and the same model holding for cryopumping. Noting equation (4.8), we may simplify (4.9) to

$$\dot{N}_c = \frac{A_p C_g (P_c - P_g)}{\sqrt{2\pi m k T_g}} \tag{4.10}$$

The theoretical maximum number of molecules per unit time colliding with A_p will occur when the condensation coefficient is unity and the evaporation coefficient is zero. Thus from equation (4.9)

$$\dot{N}_m = \frac{A_p P_c}{\sqrt{2\pi m k T_g}} \tag{4.11}$$

Defining the capture coefficient, C, as the ratio of number of molecules being captured by the cold surface to the theoretical maximum number which could be captured

$$C = \frac{\dot{N}_c}{\dot{N}_m} = C_g \left(1 - \frac{P_g}{P_c} \right) \tag{4.12}$$

To obtain experimental values of the capture coefficient, first solve equation (4.10) for the condensation coefficient

(4.13)

where $\Delta P = P_c - P_g$

and, since the number of molecules being captured is equal to the number entering through a controlled leak,

$$\dot{N}_c = \dot{N}_L \tag{4.14}$$

$$C_g = \frac{\dot{N}_L \sqrt{2\pi m k T_g}}{A_p \Delta P} \tag{4.15}$$

The capture coefficient can be determined from C_g by correcting it according to equation (4.12). The experimental quantities which must be measured are:

$\dot{N}_L$ = flow of molecules into chamber through controlled leak

T_g = the temperature of the gas, essentially the uniform temperature of the radiation shields

ΔP = the pressure drop from a steady flow condition to a no flow equilibrium.

P_g = the equilibrium pressure under no flow condition

A_p = effective area of cryopanel

4.2 Pressure Measurement

The pressure measurements are the most critical since they can incur the greatest uncertainty.

A Bayard-Alpert inverted ionization gage was utilized for all pressure measurements, both nude and envelope mounted were available. The nude gage was mounted inside the radiation shielding to eliminate conductance effects through the area in the path to the envelope mounted

gage which was installed on the wall of the tank. Radiation shielding was placed between the nude gage and the cryopanel to insure that the nude gage was seeing only the pressure of the gas in the chamber.

To understand the nature of the pressure drop, ΔP, which is evident in experimental runs, Fig. 3, the dynamics of the system must be analyzed. In this analysis a model will be proposed which will predict the experimental pressure vs. time graphs of Fig. 3.

The model of the system is shown in Fig. 4. The actual system (Fig. 9-11) is described in detail in Appendix I. The important features are the three volumes considered in the model. The large chamber is divided into an inner volume V_g, and an outer volume V_1 by the radiation shielding, which includes a cylinder with two ends. Flow areas consist of two holes for viewing on the two end shields and a clearance between cylindrical and end shields. The other volume V_e, consists of tubing leading the gas from the gas addition system to the inner volume.

All molecular fluxes considered are defined below:

$\dot{N}_L$ = Molecules/sec of controlled gas entering lines to chamber

$\dot{N}_g$ = Molecules/sec of controlled gas entering the chamber

$\dot{N}_c$ = Molecules/sec of condensable gas captured by the cryopanel

$\dot{N}_{gl}$ = Molecules/sec of gas entering the volume between radiation shields and tank walls

$\dot{N}_D$ = Molecules/sec of condensable gas pumped by the diffusion pump and cryogenic trap

$\dot{N}_{rl}$, $\dot{N}_{rg}$ = Molecules/sec of residual condensable gas leaking into chamber and from outgassing of tank walls and radiation shielding

V_e = volume of piping between gas injection stop valve and chamber

V_g = volume of chamber inside radiation shielding

V_1 = volume between radiation shielding and tank wall

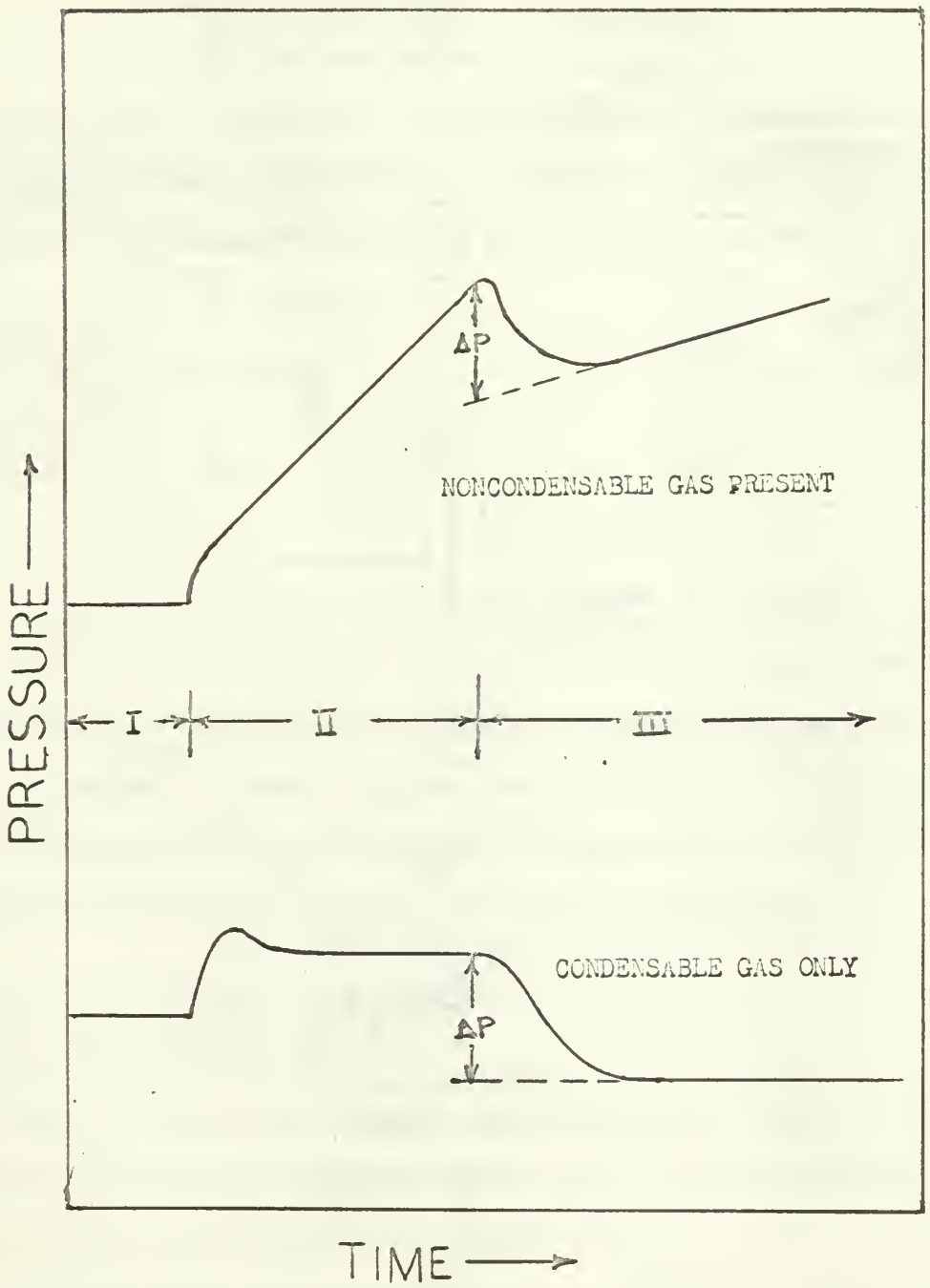

FIG. 3 EXPERIMENTAL PRESSURE VS. TIME

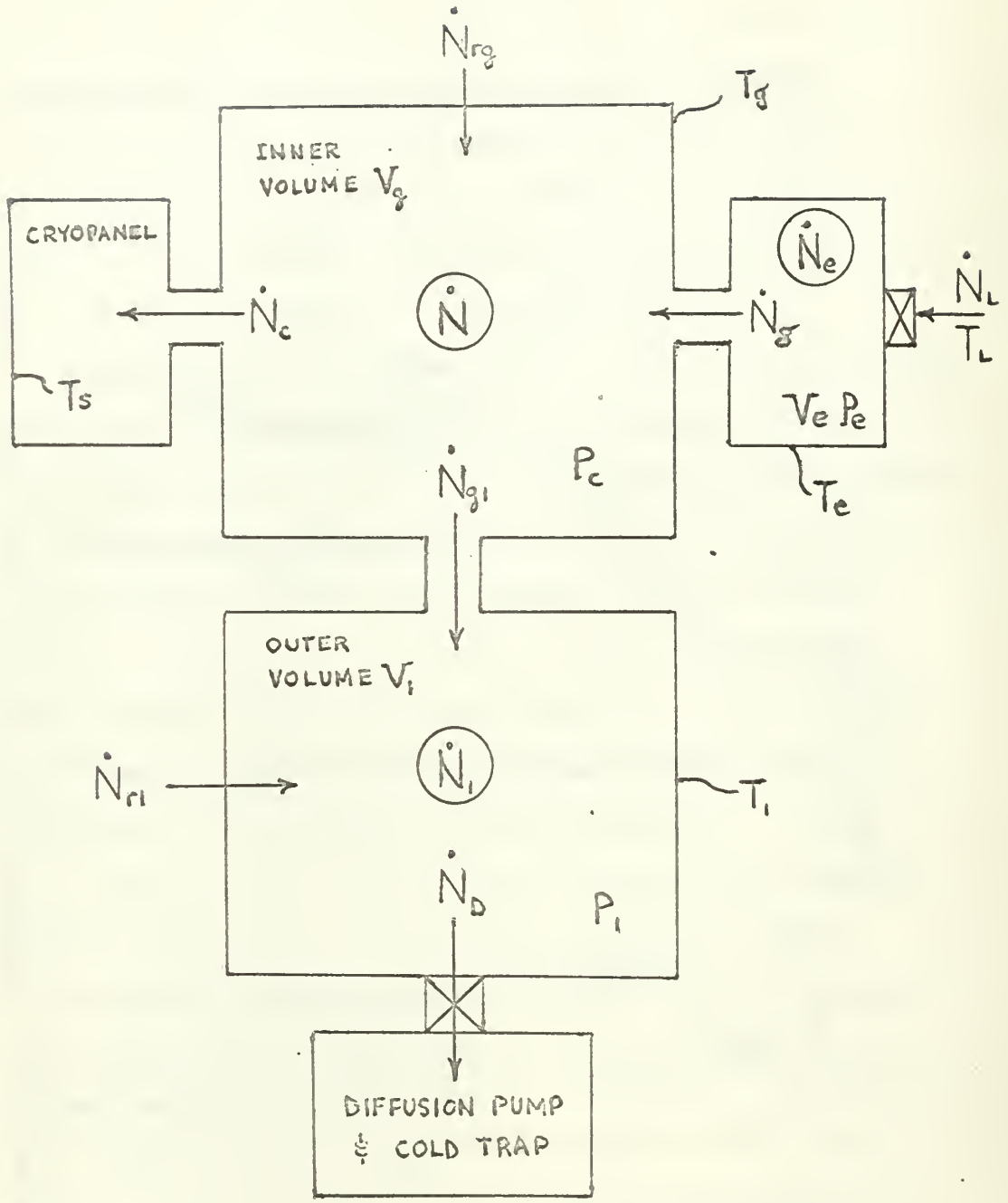

FIG. 4 CONDENSABLE GAS MODEL FOR SYSTEM DYNAMICS

T_l = mean temperature of tank wall and radiation shielding

T_e = temperature of wall piping encompassing V_e

T_L = temperature of gas admitted into V_e

(V-L) = gas injection stop valve

(V-1) = high vacuum valve to diffusion pump and cryogenic trap

A mass balance, or what is more convenient, a molecular rate balance on volume V_g of condensable gases only gives

$$\dot{N} = \dot{N}_{rg} + \dot{N}_g - \dot{N}_e - \dot{N}_{gl} \tag{4.16}$$

for V_l and V_g respectively

$$\dot{N}_l = \dot{N}_{rl} + \dot{N}_{gl} - \dot{N}_D \tag{4.17}$$

$$\dot{N}_{\ell} = \dot{N}_L - \dot{N}_g \tag{4.18}$$

In the following derivation of expressions with measurable quantities defining the above terms, it is recognized that several condensable gases may be present. By Dalton's Law, however, we may treat each gas independently. Again, this is especially true in the molecular flow regime except for the phenomena of trapping which is little understood and difficult to treat in a general analysis (2,14).

$$\dot{N} = \frac{d}{dt}\left(\frac{PVN_o}{R_M T}\right) = \frac{1}{k}\frac{d}{dt}\left(\frac{PV}{T}\right) \tag{4.19}$$

Since the gases all occupy the same unchanging volumes, and the temperature must be the same in a given volume for this analysis to hold, we can express the first term in equation (4.16)

$$\dot{N} = \frac{V_g}{kT_g}\dot{P} \tag{4.20}$$

where both N and P apply to the sum of all condensable gases. Expressions

for the first term in equations (4.17) and (4.16) are similar.

Other molecular fluxes are derived from equation (4.6) by the same type of analysis applicable to Fig. 2 except that an area cannot be assigned and, therefore, the terms before the parenthesis are lumped into a constant.

The flux of control gas into the chamber as expressed in equation (4.6)

$$\dot{N}_g = C_e \left(\frac{P_e}{\sqrt{T_e}} - \frac{P_c}{\sqrt{T_g}} \right) \tag{4.21}$$

where P_c, as defined previously, is the steady state chamber pressure for condensable gases when a gas is being continuously admitted, similarly

$$\dot{N}_{g1} = C_1 \left(\frac{P}{\sqrt{T_g}} - \frac{P_1}{\sqrt{T_1}} \right) \tag{4.22}$$

The remaining terms are considered under their physical causes.

a. Cryopanel, $\dot{N}_c$

The expression for the pumping rate on a cryopanel has been derived previously and is here repeated for clarity

$$\dot{N}_c = \frac{A_p}{\sqrt{2\pi m R}} \left(\frac{C_g P_c}{\sqrt{T_g}} - \frac{C_s P_s}{\sqrt{T_s}} \right) \tag{4.9}$$

b. Diffusion Pump and Cryogenic Trap, $\dot{N}_D$

Diffusion pumps have a fairly constant volumetric pumping rate within a broad pressure range. The characteristic curve for the diffusion pump employed including the effect of a cryogenic trap is shown in Fig. 5. From equation (4.19), for the diffusion pump only

$$\dot{N}_D = \frac{P_1}{k T_1} \dot{V}_D \tag{4.23}$$

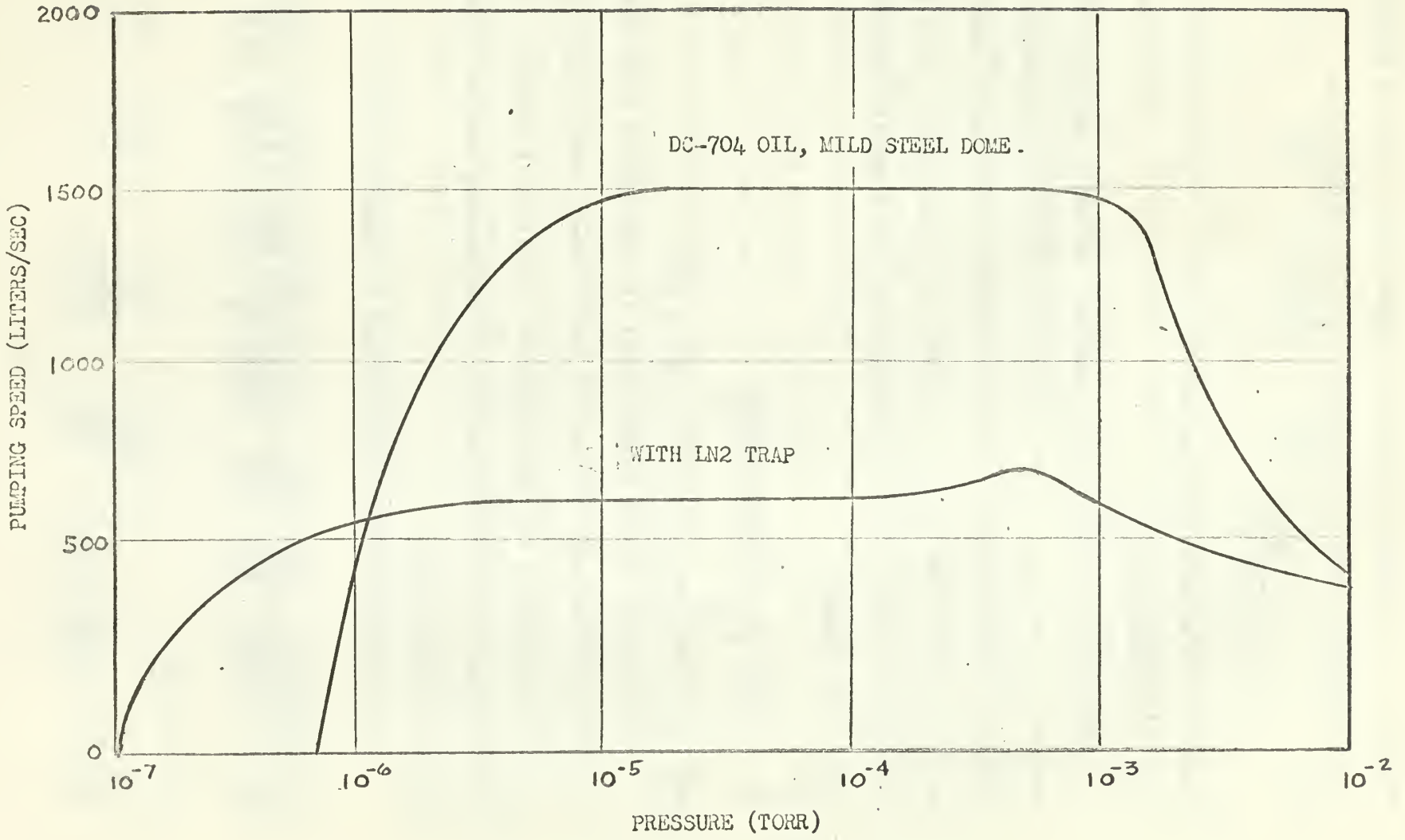

FIG. 5 DIFFUSION PUMP CHARACTERISTICS

where $\dot{V}_D$ = a constant volumetric pumping rate. When the conductance of the cryogenic trap is considered, $\dot{V}_D$ is reduced, thus

$$\dot{N}_D = \left(\frac{\alpha \dot{V}_D}{R T_1}\right) P_1 \tag{4.24}$$

where α is an efficiency factor.

c. Residual Gas, $\dot{N}_r$

Outgassing of chamber walls, gaskets, and other materials in the chamber is a continual source of gas, and although time dependent, the change is relatively slow, so that a constant source can be considered during the short time interval required for measurements. Data given is usually in terms of torr–liters/sec-cm^2 for a specific material (6). In general

$$\dot{N}_r = \frac{1}{kT_g} \frac{d}{dt}(PV) = \frac{Q_{rg}}{kT_g} \tag{4.25}$$

where Q_{rg} = outgassing rate from a given wall.

The diffusion of gas through metal is proportional to $P^{\frac{1}{2}}$ (15). Since the relative magnitude of the term is small, and changes in pressure are likewise in the same magnitude, the error in assuming a constant leakage rate should be small. The outgassing term will thus be adjusted appropriately.

Substituting the above formulations in equation (4.16)

$$\frac{V_g}{kT_g}\dot{P}_c = C_e\left(\frac{P_e}{\sqrt{T_e}} - \frac{P_c}{\sqrt{T_g}}\right) + \frac{Q_{rg}}{kT_g} - \frac{A_p}{\sqrt{2\pi mk}}\left(\frac{C_g P_c}{\sqrt{T_g}} - \frac{C_s P_s}{\sqrt{T_s}}\right) - C_1\left(\frac{P_c}{\sqrt{T_g}} - \frac{P_1}{\sqrt{T_1}}\right) \tag{4.26}$$

in eq. (4-17)

$$\frac{V_1}{RT_1}P_1 = C_1\left(\frac{P_c}{\sqrt{T_g}} - \frac{P_1}{\sqrt{T_1}}\right) + \frac{Q_{r1}}{kT_1} - \frac{\alpha \dot{V}_D}{kT_1}P_1 \tag{4.27}$$

in eq. (4-28)

$$\frac{V_e}{kT_e}\dot{P}_e = \frac{Q_L}{kT_L} - C_e\left(\frac{P_e}{\sqrt{T_e}} - \frac{P_c}{\sqrt{T_g}}\right) \qquad (4\text{-}28)$$

The total pressure P is the sum of the partial pressures of all the condensable gases. The partial pressure of each condensable gas is different because each gas cryopumped has a different theoretical pumping speed and condensation coefficient.

However, considering only changes for the gas of interest, other condensable gases will have no effect on the pressure change unless their concentrations are disturbed. Since all of these concentrations are not known and only the total pressure is measured, the partial pressure of the test gas cannot be known. A measurement of $\Delta P = P_c - P_g$ is possible for the gas of interest above, but a measurement of P_g is not possible for the controlled gas without a mass spectrometer. The equilibrium pressure reached after the controlled leak has been shut off is given by eq. (4.8) for only one condensable gas. Since the ionization gage measures total pressure, the equilibrium pressure measured under no flow conditions is P_g only if all other condensable gases are considered to be present in negligible quantities. Making this approximation, and with $P = P_c$, eq. (4.26), (4.27), (4.28) are re-expressed

$$\dot{P}_c = \frac{Q_{rr}}{V_g} + C_c\frac{A_p}{V_g}\sqrt{\frac{kT_gP_s}{2\pi m}} + \frac{C_kT_g}{V_g\sqrt{T_i}}P_i + \frac{C_kT_g}{V_g\sqrt{T_e}}P_e - \left(\frac{C_kT_g}{V_g\sqrt{T_g}} + C_g\frac{A_p}{V_g}\sqrt{\frac{kT_g}{2\pi m}} + \frac{C_iKT_g}{V_g\sqrt{T_g}}\right)P_c \qquad (4.29)$$

$$\dot{P}_i = \frac{Q_{rr}}{V_i} + \frac{C_iKT_i}{V_i\sqrt{T_g}}P_c - \left(\frac{\alpha\dot{V}_p}{V_i} + \frac{C_iKT_i}{V_i\sqrt{T_i}}\right)P_i \qquad (4.30)$$

$$\dot{P}_e = \frac{Q_L}{V_e}\frac{T_e}{T_L} + \frac{C_e k T_e}{V_e\sqrt{T_g}} P_c - \frac{C_e k T_e}{V_e\sqrt{T_e}} P_e \tag{4.31}$$

The above expressions can be simplified by defining appropriate constant factors given in Table I.

$$\dot{P}_c = (\tilde{\pi}_1 + \tilde{\pi}_2) + a_1 P_1 + a_2 P_e - (a_3 + a_4 + a_5) P_c \tag{4.32}$$

$$\dot{P}_1 = \tilde{\pi}_3 + a_6 P_c - (a_7 + a_8) P_1 \tag{4.33}$$

$$\dot{P}_e = \tilde{\pi}_4 + a_9 P_c - a_{10} P_e \tag{4.34}$$

The above equations which represent the dynamics of the system of Fig. 4 can be solved analytically, or the system can be simulated by the use of analog computer techniques to allow flexibility in adjustment of system parameters as has been accomplished in Appendix VII.

The solution of the above equations are given for the following regions as specified in Fig. 3.

a. Region I. High vacuum value open to diffusion pump, gas flow into V_g

$$P_c(I) = \frac{(a_7 + a_8)(\tilde{\pi}_1 + \tilde{\pi}_2) + a_1 a_{10}\tilde{\pi}_3 + a_2(a_7 + a_8)\tilde{\pi}_4}{(a_3 + a_4 + a_5)(a_7 + a_8)a_{10} - a_1 a_6 a_{10} - a_2 a_4 (a_7 + a_8)} \tag{4.34}$$

$$P_1(I) = \left(\frac{a_6}{a_7 + a_8}\right) P_c(I) + \left(\frac{\tilde{\pi}_3}{a_7 + a_8}\right) \tag{4.35}$$

TABLE I COEFFICIENTS OF DYNAMIC EQUATIONS

COEFFICIENT	EXPRESSION	COEFFICIENT	EXPRESSION
π_1	Q_{rg} / V_g	a_4	$C_g \left(\frac{A_p}{V_g}\right) \frac{kT_g}{\sqrt{2\pi m k T_g}}$
π_2	$C_e \left(\frac{A_p}{V_g}\right) \frac{kT_g}{\sqrt{2\pi m k T_s}} \frac{P_s}{}$	a_5	$\frac{C_i k \sqrt{T_g}}{V_g}$
π_3	Q_{ri} / V_i	a_6	$\frac{C_i k \sqrt{T_i}}{V_i} \sqrt{\frac{T_i}{T_g}}$
π_4	$\frac{Q_L}{V_e} \left(\frac{T_e}{T_L}\right)$	a_7	$\alpha \dot{V}_D / V_i$
a_1	$\frac{C_i k \sqrt{T_g}}{V_g} \sqrt{\frac{T_g}{T_i}}$	a_8	$\frac{C_i k \sqrt{T_i}}{V_i}$
a_2	$\frac{C_e k \sqrt{T_g}}{V_g} \sqrt{\frac{T_g}{T_e}}$	a_9	$\frac{C_e k \sqrt{T_e}}{V_e} \sqrt{\frac{T_e}{T_g}}$
a_3	$\frac{C_e k \sqrt{T_g}}{V_g}$ —	a_{10}	$\frac{C_e k \sqrt{T_e}}{V_e}$

$$P_e(I) = \left(\frac{a_9}{a_{10}}\right) P_c(I) + \left(\frac{\pi_4}{a_{10}}\right) \tag{4.36}$$

Since all constants are positive real numbers, both $P_I(I)$ and $P_e(I)$ are above $P_c(I)$ by the given factors. All three pressures can be measured experimentally.

b. Region II. High vacuum value is closed to diffusion pump; gas flow into V_g continues.

The transient effect is tedius to solve analytically for the third order system above without numerical values. The analog computer solution is shown in Fig. 6. Equilibrium values are readily solved since the only effect is that $a_7 = 0$

$$P_c(II) = \frac{a_8(\pi_1 + \pi_2) + a_1 a_{10} \pi_3 + a_2 a_8 \pi_4}{a_8(a_3 + a_4 + a_5) - a_1 a_6 a_{10} - a_2 a_4 a_8} \tag{4.37}$$

$$P_I(II) = \left(\frac{a_6}{a_8}\right) P_c(II) + \left(\frac{\pi_3}{\pi_8}\right) \tag{4.38}$$

$$P_e(II) = \left(\frac{a_9}{a_{10}}\right) P_c(II) + \left(\frac{\pi_4}{a_{10}}\right) \tag{4.39}$$

c. Region III. Gas flow into V_g is stopped.

Again, transient effects are shown in Fig. 6. The effect of the gas injection value closing time can alter the shape of the decay curve considerably. Equilibrium values are obtained for $\pi_4 = 0$

$$P_c(III) = \frac{a_8(\pi_1 + \pi_2) + a_1 a_{10} \pi_3}{a_8(a_3 + a_4 + a_5) - a_1 a_6 a_{10} - a_2 a_4 a_8} \tag{4.40}$$

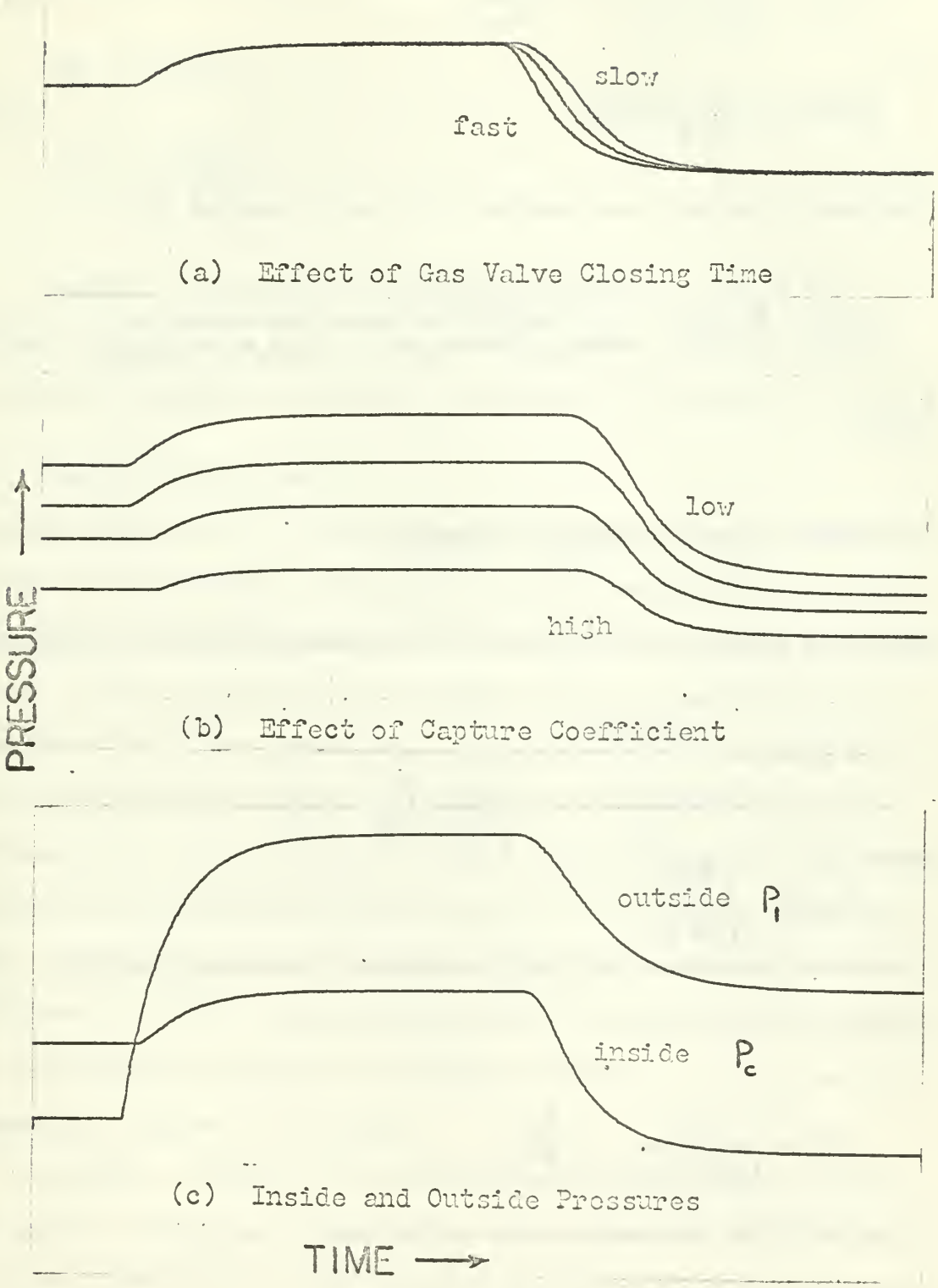

FIG. 6 MODEL SOLUTION OF PRESSURE VS. TIME

$$P_1(III) = \left(\frac{a_6}{a_8}\right) P_c(III) + \left(\frac{\pi_3}{a_8}\right) \tag{4.41}$$

$$P_e(III) = \left(\frac{a_9}{a_{10}}\right) P_c(III) \tag{4.42}$$

The result from the above analysis which is of interest is

$$P_c(II) - P_c(III) = \frac{a_2 a_8 \pi_4}{a_8 a_{10}(a_3 + a_4 + a_5) - a_1 a_6 a_{10} - a_2 a_8 a_{10}} \tag{4.43}$$

since

$$\Delta P = P_g - P_c = P_c(II) - P_c(III) \tag{4.44}$$

and after substituting the appropriate expressions from the coefficients

$$\Delta P = \frac{Q_L / T_L}{C_g \frac{A_p S_{th}}{T_g} + \frac{C_1 k}{\sqrt{T_g}}\left(\sqrt{\frac{T_1}{T_g}} - 1\right)} \tag{4.45}$$

where

$$S_{th} = \sqrt{\frac{R_M T_g}{2\pi M}}$$

the above formulation for ΔP includes all temperature effects. For $T_1 = T_g$

$$\Delta P = \frac{Q_L}{C_g A_p S_{th}} \left(\frac{T_g}{T_L}\right) \tag{4.46}$$

if we solve for the condensation coefficient

$$C_g = \frac{Q_L}{\Delta P A_p S_{th}} \left(\frac{T_g}{T_L}\right) \tag{4.47}$$

The above equation is now equivalent to equation (4.15) for

$$Q_L = \dot{N}_L k T_L \tag{4.48}$$

$$S_{th} = \sqrt{\frac{2\pi m}{k T_g}} \tag{4.49}$$

Therefore, the pressure drop actually measured is indeed the pressure drop desired from eq. (4.15) for obtaining the condensation coefficient provided the appropriate temperature corrections are applied.

4.3 Temperature Measurement

The temperatures of interest are: the temperature of the gas before entering the tubulation to the chamber T_L, the temperature of the cryosurface T_s, and the temperature of the gas T_g, which impinges on the cryopanel. In the free molecular flow regime where the mean free path is many times the chamber dimensions, the gas molecules can be made to collide with the tank surface or radiation shield before striking the cryopanel if the ratio of the area of the radiation shield to that of the cryopanel is maintained sufficiently high ($>$ 10). Thus, the temperature of the gas T_g, will be essentially that of the radiation shields. It is important to have a uniform temperature or there will not be a Maxwellian distribution, and molecular streaming will occur, in which case the macroscopic approach is not valid.

Similarly, all areas of the cryosurface must be within 1-2°K since the capture coefficient changes sharply with temperature for CO_2 and N_2 at about 15-20°K (20). As the surface becomes coated with the condensate a local increase in temperature will greatly increase the vapor pressure

at that area, thereby decreasing overall cryopumping.

4.4 Cryosurface Area

Since the cryosurface area enters into the computation of the capture coefficient, an accurate determination is necessary. The most effective method employed is to use a surface of simple geometry, a sphere, for example, and vacuum insulated cryogenic lines to the surface. In the system employed in this experiment a commerical cryopanel was used and, although one side is flat (Fig 12), the other side is raised and an estimate must be made of its actual surface area. The projected area was used for calculation purposes resulting in an uncertainty. Another difficulty was encountered in the construction of vacuum insulated lines. Because of a peculiarity in the system, a vacuum jacket could not be installed without a great deal of redesign and construction. Considering the time available and other requirements, it was decided to provide a thermal shield around the supply and return lines. The equilibrium temperature of this shield can be calculated considering radiation exchange between two infinite parallel plates (the cryogenic line and tank wall) having the same emissivity with a thin radiation shield between them (16).

$$T_3^4 = \tfrac{1}{2}\left(T_1^4 + T_2^4\right) \tag{4.50}$$

for $T_1 = 20°K$, $T_2 = 77°K$ $\quad T_3 = 65°K$

4.5 Flow Measurement

The remaining measurement, the flow rate of gas admitted, was accomplished by measuring the pressure rise in a known volume and is discussed in detail in Appendix III. Research quality gas of the highest

purity was employed to minimize other non-condensables being injected into the system, but leakage through the flow control system may cause contamination by condensables. The flow was deflected by two plates as it entered the chamber in order to insure diffuse flow in the chamber and avoid possible streaming.

5. Experimental Results

Condensation coefficients for 300°K CO_2 are reported in tabular form in Table II showing both flow rates and pressure drops obtained. Calculation of the condensation coefficients is discussed in detail in Appendix V.

The condensation coefficients for CO_2 are also plotted as functions of ΔP and Q_L in Figs. 7 and 8, to emphasize a functional relationship with the flow measurement technique and effect of vapor pressure as discussed in the following section.

The condensation coefficients for 300°K N_2 are presented in tabular form in Table III. Although those points were not plotted as with CO_2, the same relationships with ΔP and Q_L apply.

TABLE II RESULTS OF CRYOPUMPING CO_2

RUN	ΔP TORR x 10^6	Q_L TORR-LITERS/SEC.	C_g
1	0.30	.0060	.90
2	2.20	.0184	.38
3	1.15	.0148	.60
4	0.40	.0068	.78
5	3.20	.0224	.34
6	2.55	.0192	.35
7	1.50	.0156	.48
8	0.80	.0120	.69
9	1.00	.0168	.78
10	1.10	.0120	.50

$T_g = 296 \pm 2\ ^oK$

$T_s = 85.7 \pm 1.3\ ^oK$

$(C_g)_{ave} = .58 \pm .18$

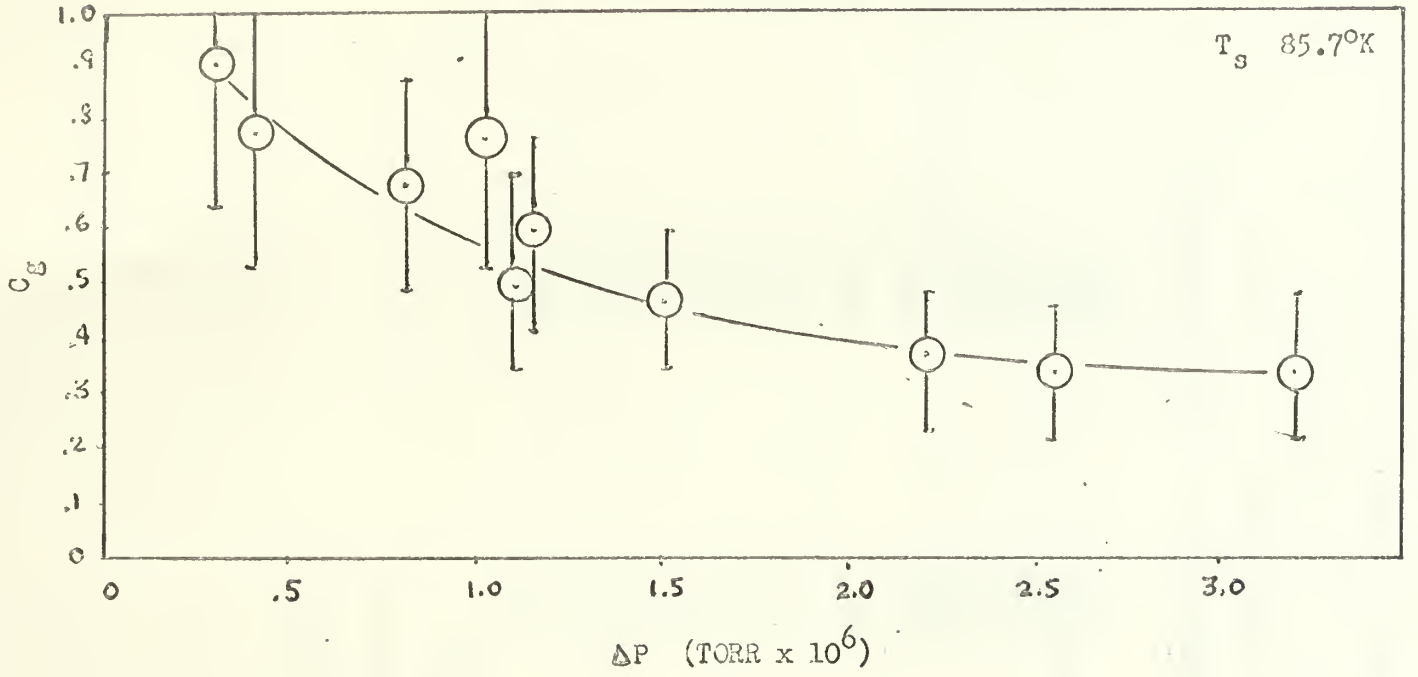

FIG. 7 CONDENSATION COEFFICIENTS FOR 300°K CO_2

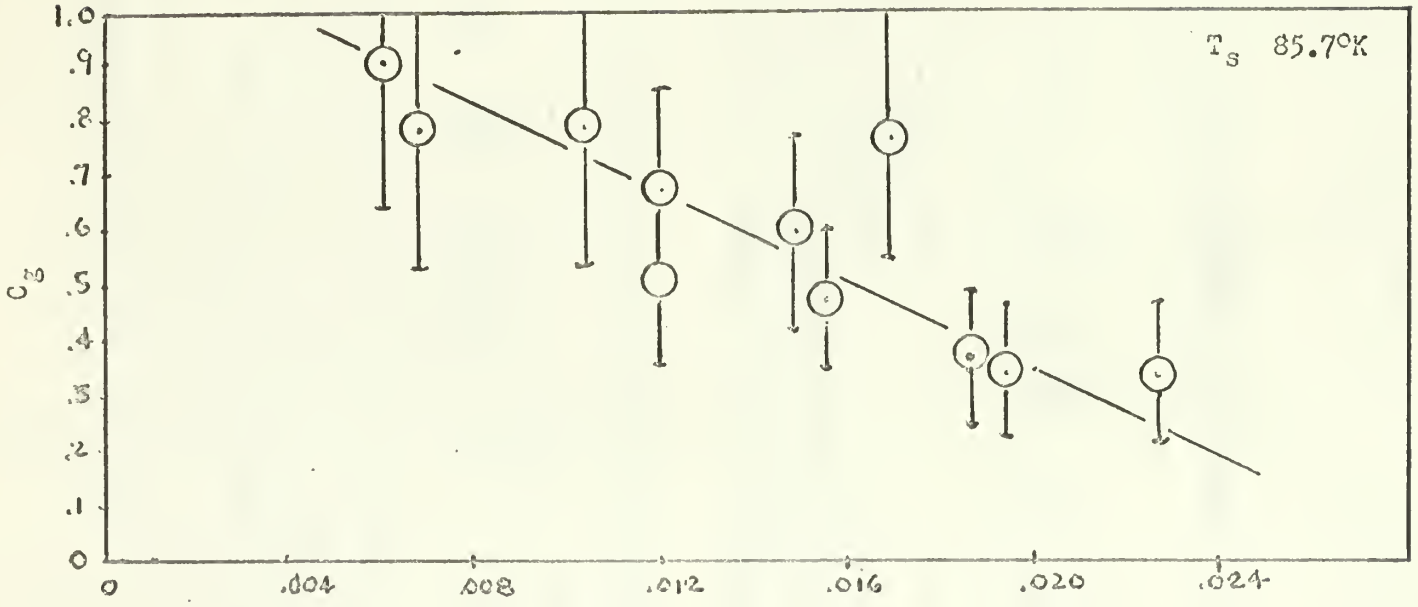

FIG. 8 CONDENSATION COEFFICIENTS FOR 300°K CO_2

TABLE III RESULTS OF CRYOPUMPING N_2

RUN	ΔP TORR x 10^7	Q_L TORR-LITERS/SEC.	C_g
1	4.9	.00920	.50
2	1.5	.00400	.71
3	1.1	.00296	.72
4	1.6	.00400	.67

$T_g = 294 \pm 2\,^{\circ}K$

$T_s = 32.5 \pm 3.3\,^{\circ}K$

$(C_g)_{ave} = .65 \pm .20$

6. Discussion of Results

6.1 Error Analysis

An analysis of the error involved in measuring the capture coefficient must involve all fundamental measurements. The working formulas for calculating the capture coefficient are from eq. (4.47) and eq. (4.12) repeated here:

$$C_g = \frac{Q_L}{\Delta P\, A_p\, S_{th}} \left(\frac{T_g}{T_L}\right) \tag{6.1}$$

$$C = C_g \left(1 - \frac{P_g}{P_c}\right) = C_g \frac{\Delta P}{P_c} \tag{6.2}$$

where $Q_L = \dot{P}_L V_L$

$$S_{th} = \sqrt{\frac{R_M T_g}{2\pi M}}$$

Since the pressure drop is measuredby an ionization gage, the observed measurement must be corrected by the ionization gage sensitivity, .

Thus, eq. (6.1) becomes, including all fundamental measurements,

$$C_g = \frac{2\pi M}{R_M} \frac{\dot{P}_L V_L \gamma}{A_p \Delta P_M} \left(\frac{T_g}{T_L}\right)^{1/2} \tag{6.3}$$

The pressure of the test gas by itself cannot be measured without a mass spectometer; only the condensation coefficient, C_g, will be reported. Values of the capture coefficients reported in the literature are measured under the assumption that $P_c \gg P_g$; therefore, comparisons of the condensation coefficients are valid.

Uncertainties for each measurement are tabulated below:

TABLE IV

Uncertainty in Measured Values

QUANTITY	UNCERTAINTY	FRACTION
P_L	Variable	.25
V_L	1 cc	.0125
	.2	.146
A_p	300 cm^2	.104
	Variable	.05
T_g	2°K	.0015
T_L	2°K	.0015

The uncertainty for P_L is due to the fact that the slope of pressure vs. time graph as shown in Fig. 19 should be taken at P_e obtained during steady state flow. The slope was actually measured at 300 μ , leading to a higher flow rate. A percentage error was assumed from approximate knowledge of equilibrium P_e.

The uncertainty in ΔP is due to the non-linearity in response of the ionization gage and collecter current to actual pressure scale factor; the pressure calibration is considered in the sensitivity of the gage. The smallest division on each scale is .02 x full scale values. A maximum error is scaling of .2 over 4.0 full division was observed thus the fractional error is .05 ΔP

Employing the error analysis for a single sample experiment where each variable is assumed to be normally distributed (19)

$$\left(\frac{\Delta C_g}{C_g}\right)^2 = \left(\frac{\Delta \dot{P}_L}{P_L}\right)^2 + \left(\frac{\Delta V_L}{V_L}\right)^2 + \left(\frac{\Delta A_p}{A_p}\right)^2 + \left(\frac{\Delta(\Delta p)}{\Delta P}\right)^2 + \left(\frac{\Delta T_L}{T_L}\right)^2 + \frac{1}{4}\left(\frac{\Delta T_g}{T_g}\right)^2 + \left(\frac{\Delta \gamma}{\gamma}\right)^2 \quad (6.4)$$

Substituting the above values

$$\frac{\Delta C_q}{C_q} = .312 \tag{6.5}$$

If P_e was known for each run then $\frac{\Delta \dot{P}}{\dot{P}} = .10$ and the uncertainty in the condensation coefficient would be reduced considerably

$$\frac{\Delta C_q}{C_q} = .222 \tag{6.6}$$

6.2 Comparison with Published Data

The resulting average condensation coefficients compare well with data published by ARO and by Albero in previous research at this school.

TABLE V

Comparative Data on Capture Coefficients

	GAS TEMP	CRYOSURFACE TEMP	CAPTURE COEFF.	REFERENCE
	°K	°K		
CO_2	300	77	0.64	(12)
	300	77	0.70	(18)
	296	86°K	0.58	
N_2	300	22.6	0.61	(20)
	294	32.5	0.65	

The uncertainties involved fully account for the differences in reported capture coefficients.

The system employed for measuring capture coefficients can be improved to reduce all the uncertainties and an experimental error in the capture coefficient approaching .07, as estimated in the report from ARO, can be attained (20).

7. Conclusions

The capture coefficients of CO_2 and N_2 were measured employing the pressure drop method. An analysis of the method and experimental procedure placed a 31.2% uncertainty on the results.

The use of the pressure drop method requires temperature corrections as concluded from an analysis of the system, and it is limited in that it can measure only a large fraction of the partial pressure of the test gas. However, values reported for the capture coefficient assume that the partial pressures of other condensable and non-condensable gases are small. Without this approximation the condensation coefficient is being actually reported. Thus, the values reported in this research are truly condensation coefficients.

Upon further refinement of flow and pressure measurement techniques, a considerable reduction in uncertainty is expected.

The present system has been analyzed and simulated so that temperature corrections and measurement of the pressure drop necessary to calculate the condensation coefficient are clearly defined.

The construction of Helium transfer lines and control console has adapted the system to a Helium refrigerator and consolidated necessary instrumentation for an efficient data gathering process.

BIBLIOGRAPHY

1. Bailey, B. M., and Chaun, R. L., 1958 Vacuum Symposium Transactions, 262, Pergamon Press, Inc., 1959.

2. Wang, E. S. J., Collins, J. A. Jr., and Haygood, J. D., "General Cryopumping Study", Advances in Cryogenic Engineering, Vol. 7, Plenum Press, 1962.

3. Chaun, R. L., and Wallace, D., "Present Status of Cryopumping", USEC Memorandum No. 1, November, 1960.

4. Brown, R. F., and Wang, E. S. J., "Capture Coefficients of Gases at 77°K", Advances in Cryogenic Engineering, Vol. 10, Plenum Press, 1965.

5. Dawson, J. P., and Haygood, J. D., "Cryopumping", Cryogenics, Vol. 5, p. 57, No. 2, April, 1965.

6. Dushman, S., Scientific Foundations of Vacuum Technique, 2nd Edition, John Wiley & Sons, Inc., New York, 1962.

7. John, J. E. A., and Hardgrove, W. F., "Cryosorption-A Method for Simulating the Space Vacuum Environment, "Technical Report, GSFC 322-Y-09-04, January, 1965.

8. Cheng, D., and Simson, J. P., "Obtaining Low Pressures with Cryosorption Pumps", Advances in Cryogenic Engineering, 292, Vol. 10, Plenum Press, New York, 1965.

9. Lennard-Jones, J. E., and Devonshire, A. F., "The Interaction of Atoms and Molecules with Solid Surfaces", Part III, Proc. Royal Society (London), Ser. A 156, No. A, August, 1936.

10. Part IV of reference 9.

11. Buffham, B. A., Henault, P. B., and Flinn, R. A., "A Theoretical Evaluation of the Sticking Coefficient in Cryopumping", 1962 Vacuum Symposium Transactions, 205, Pergamon Press, Inc., 1963.

12. Dawson, J. P., Haygood, J. D., "Temperature Effects on the Capture Coefficient of CO2", AEDC-TDR-63-251, January, 1964.

13. Haygood, J. D., and Dawson, J. P., "Considerations in the Measurement of Cryopumping Capture Coefficients", AEDC-TR-65-68, April, 1965.

14. Hemstreet, R. A., et al., "Research Study of the Cryotrapping of Helium and Hydrogen During 20°K Condensation of Gases, Phases I and II", AEDC-TDR-63-127, May, 1963.

15. Scott, R. B., Cryogenic Engineering, New Jersey, D. Van Nostrand Company, Inc., 1959.

16. Chapman, A. J., Heat Transfer, The MacMillan Co., New York, 1960.

17. LaChance, G. M., "The Theory and Construction of a Liquid Helium Cryopump", thesis, U. S. Naval Postgraduate School, 1964.

18. Albero, C. M., "Design and Development of a Cryogenic Pumping Evaluation Facility", Thesis, U. S. Naval Postgraduate School, 1965.

19. Kline, S. J., and McClintock, F. A., "Uncertainties in Single-Sample Experiments", Mechanical Engineering, January, 1953.

20. Dawson, J. P., "Temperature Effects on the Capture Coefficients of Six Common Gases", AEDC-TDR-64-84, May, 1964.

21. Sreekanth, A. K., Advances in Applied Mechanics, Rarefied Gas Dynamics, Vol. 1, 621, Academic Press, New York, 1965.

22. Powell, R. L. and Sparks, L. L., "Available Low Temperature Thermocouple Information and Services", NBS Report 8750, February, 1965.

APPENDIX I

General Description of System

The basic system employed for this investigation is a modified 40 inch diameter vacuum furnace manufactured by National Research Corporation. Modifications and improvements on the system were performed by previous investigators, LT G. M. LaChance and LT C. M. Albero (17, 18). A schematic and photographs of the present system are shown in Figs. 9-11.

This year, the equipment was moved to a newly established Cryogenic Laboratory at the U. S. Naval Postgraduate School and appropriate modifications were made to incorporate the use of an A.D. Little Helium Refrigerator and to obtain data on capture coefficients from a commercially produced cryopanel. These modifications are described in detail below.

a. The cryopanel installed shown in Fig. 12 was constructed by Dean Products utilizing their single embossing technique. The two 12x20" sheets of 16 gage 304 stainless steel are edge sealwelded along the periphery of the panel. The panel is electropolished and tested to a leak rate not exceeding 1×10^{-8} std cc/sec of Helium. The flat side of the panel faces the forward viewport located above the control panel.

b. All necessary electrical controls were consolidated in a desk top panel. A line diagram of the electrical network is shown in Figs. 15, 16. The use of controllers for power to valve solenoids insures that the diffusion pump will be isolated in the event of a power failure since the fore pump would not be operating. In the controller for the diffusion pump, a thermal switch and an overpressure relay are in series with the trip out coils to protect the diffusion pump against overheating,

and thus breaking down the oil, and also against prolonged exposure to atmospheric pressure. The overpressure relay is activated by the ionization gage and trips at a pressure of approximately 130% of full scale of that scale set on the ionization gage controller. An overpressure relay by-pass is necessary in startup and during normal operation since the diffusion pump would otherwise trip out each time the filament on the ionization gage is turned off for a zero check. Detailed operation of the system is discussed in Appendix II .

c. Viewports were installed on both ends of the tank for visual observation. A 4" diameter 1056 glass disc sealed to a Kovar sleeve was welded to a stainless steel ring which was then welded to the chamber as shown in Fig. 13. This measure was necessary as difficulty was first experienced when the Kovar was welded by inert gas welding directly to the tank. A view of the cryopanel as seen from the forward viewport is shown in Fig. 12. An incandescent 200 watt light was fitted in an enclosure provided with a ventilation fan and mounted on the rear viewport to provide interior lighting. Since the panel and thermal shields are electro-polished, sufficient light was reflected to the forward face of the panel to allow visual observation. The nude ionization gage actually provided a good source of light for visual observation when operating at 10 ma filament current.

d. A Liquid Nitrogen transfer system was installed to fill the radiation shield, cryopanel, and cryogenic trap above the diffusion pump. A 50 liter dewar feeds 3/8" Nylon lines which are insulated with a 3/4" thick foam rubber Armaflex insulation. Jamesbury quarter turn cryogenic valves stop the flow to each of three sections to the radiation shield. An automatic level controller was employed for filling the cryogenic

trap.

The use of flared fittings and Nylaflow hose has proved satisfactory.

By ensuring a tight fit over the supply lines and insulating the exhaust lines, equilibrium temperature was reached on the cryopanel within 30 minutes. Pressurizing the dewar with He at 8 psi maintained a steady flow of nitrogen to the panel and a uniform temperature on the panel. For a 300°K wall this flow is approximately 2 liters per hour.

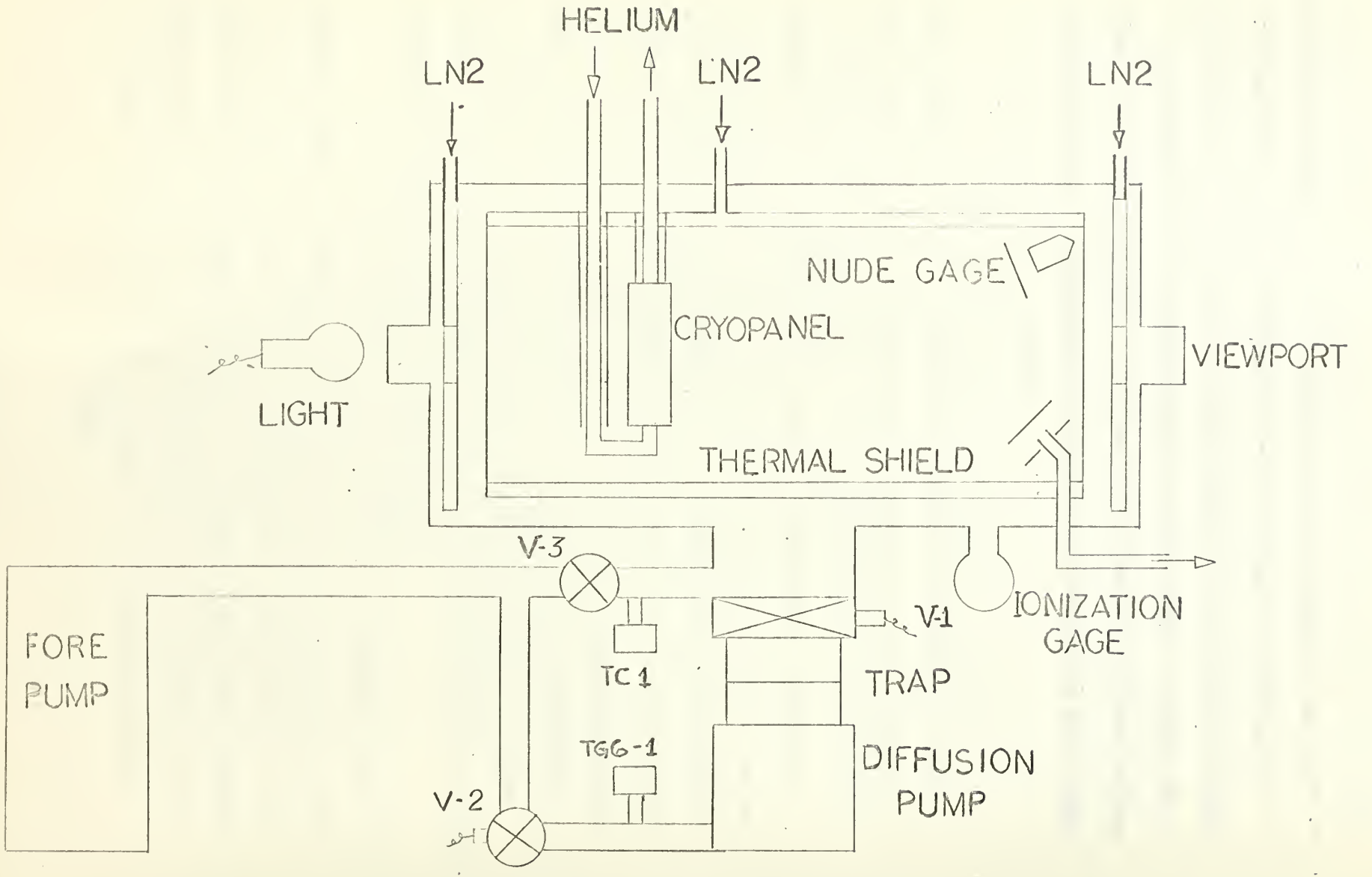

FIG. 9 SCHEMATIC OF SYSTEM

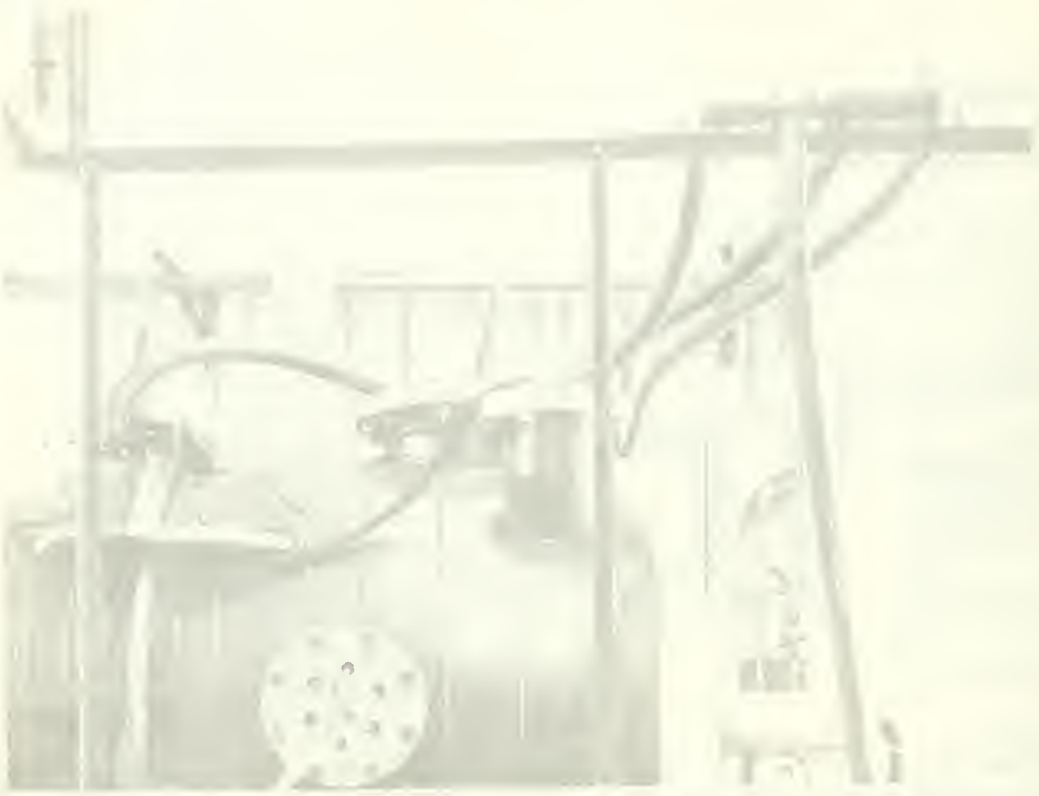

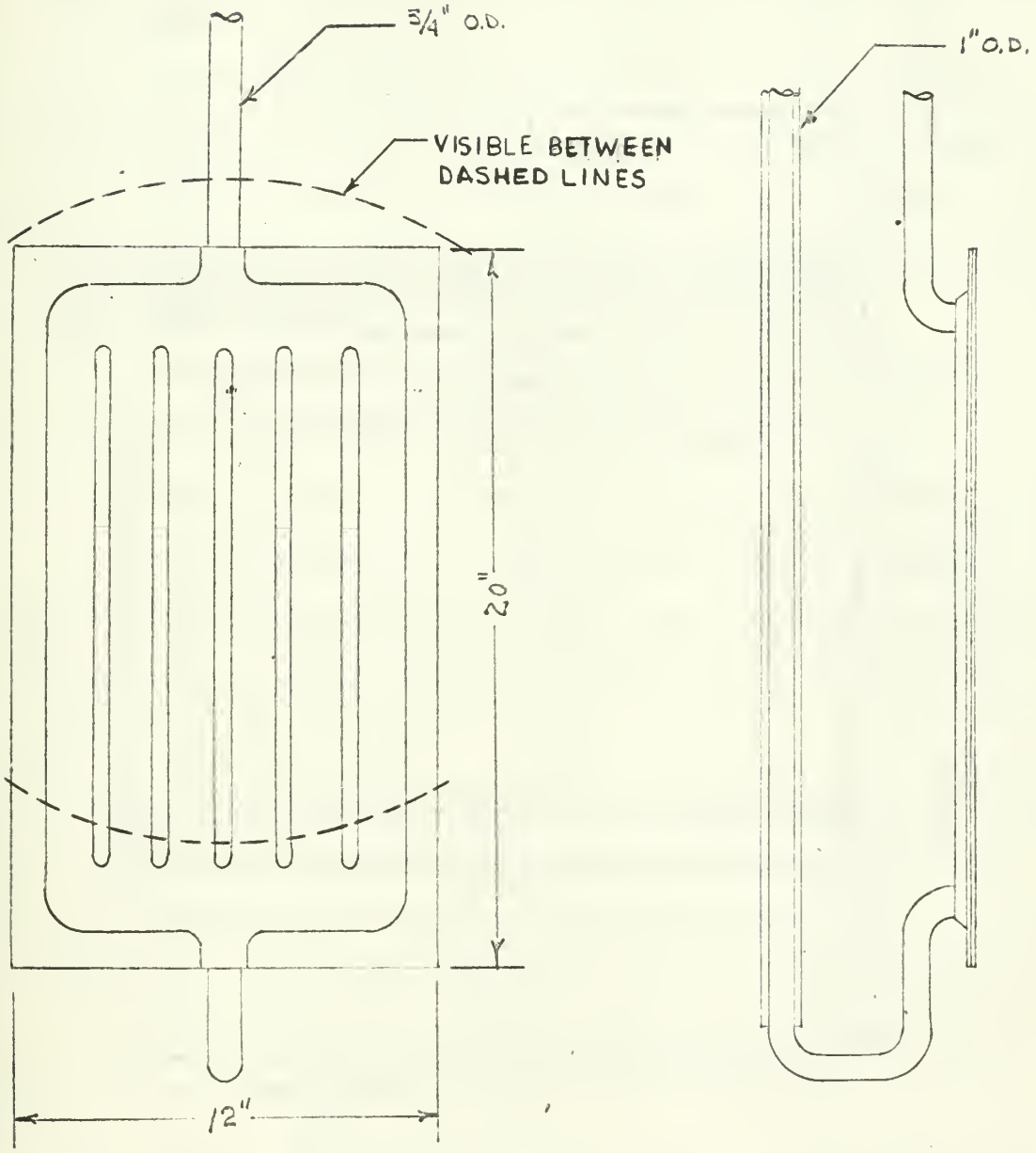

FIG. 12 CRYOPANEL

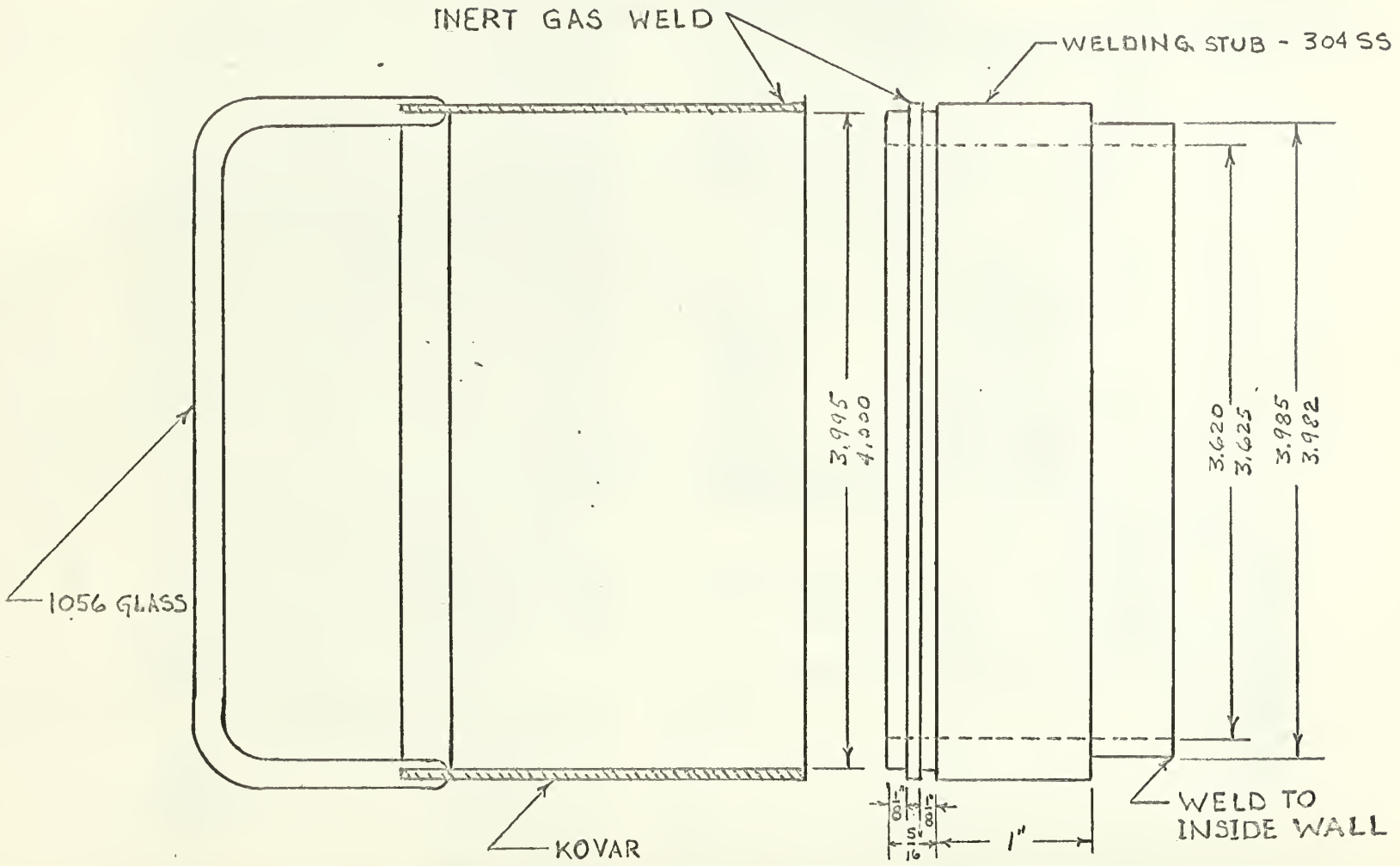

FIG. 13 WINDOW ASSEMBLY

APPENDIX II

Operating Procedure

Vacuum System (See Figures 9, 14, 15)

1. Check oil in lubricating caps and in sight glass on roughing pump.
2. Close disconnect and controller switch for roughing pump.
3. Close breaker and controller switches for solenoid valves and diffusion pump. Open both valves for air supply to pneumatic valves. Meter on panel should indicate air pressure of 90 psi.
4. Valves automatically close upon loss of electrical power.
5. Insure both vent valves are closed tightly.
6. Turn on power to solenoids and open high vacuum valve (V-1), foreline valve (V-2). Open roughing valve (V-1) manually.
7. Open degassing valve on roughing pump slightly and start pump.
8. Monitor tank pressure on TC-1 and foreline pressure on TG-6 position 1.
9. When tank pressure reaches 70 μ start diffusion pump. Overpressure protection switch should be on "out". Water to diffusion pump need not be turned on at this time.
10. When tank pressure reaches 30 μ close the roughing valve (V-3). This is to prevent backstreaming of roughing pump oil into chamber.
11. Monitor temperature of diffusion pump by hand. In about 20 minutes, when hot,open cooling water valve to diffusion pump.

Insure that quick cool-down valve is closed.

12. A momentary rise in foreline pressure and a rapid decrease in tank pressure will be noticed when diffusion pump is in full operation.

13. When pressure is below 10^{-4} torr, fill cryogenic trap with LN_2 to prevent backstreaming of diffusion pump oil.

14. Operation of ionization gage is outlined in manual, however, gage needs to be degassed and zero adjusted periodically. When leaving system turn overpressure protection switch to "in" position to prevent extended exposure of diffusion pump to high pressure. Trip is set at 130% full scale.

Cryogenic System

1. When 50 liter dewar is full, insert stainless steel draw tube with relief valve, and connect to cryogenic line with rubber tubing.
2. Pressurize dewar with 6-8 psig of Helium to maintain a steady flow to cryopanel or shields.
3. Insure that Armaflex connection fits tight around supply and exhaust lines to shields and cryopanels.
4. Open quarter turn valves about half way and observe exhaust.
5. Monitor thermocouples for uniformity of temperature.
6. It will be necessary to maintain a flow of liquid out of the exhaust in order to maintain uniform temperatures.

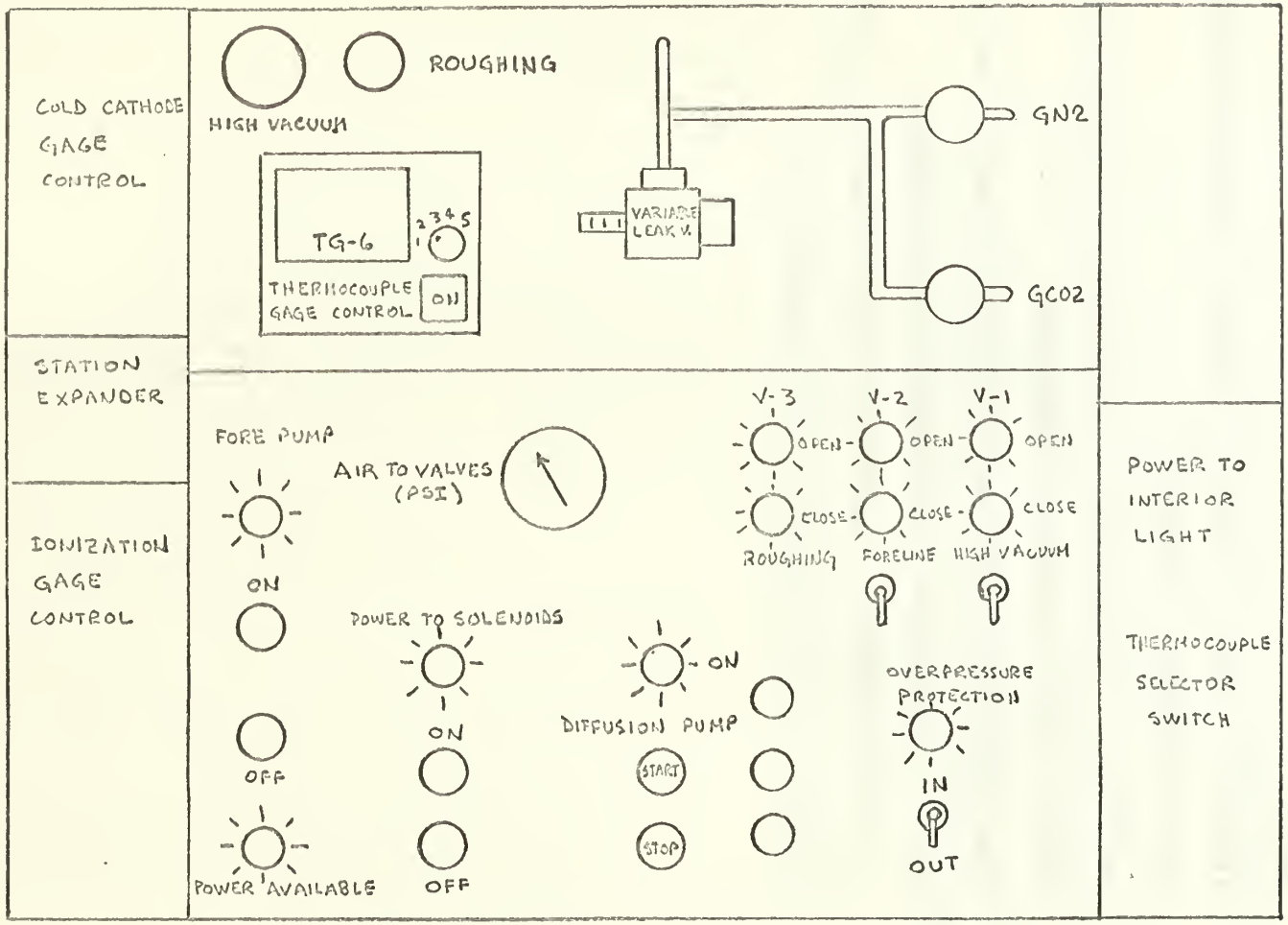

FIG. 14 CONTROL PANEL

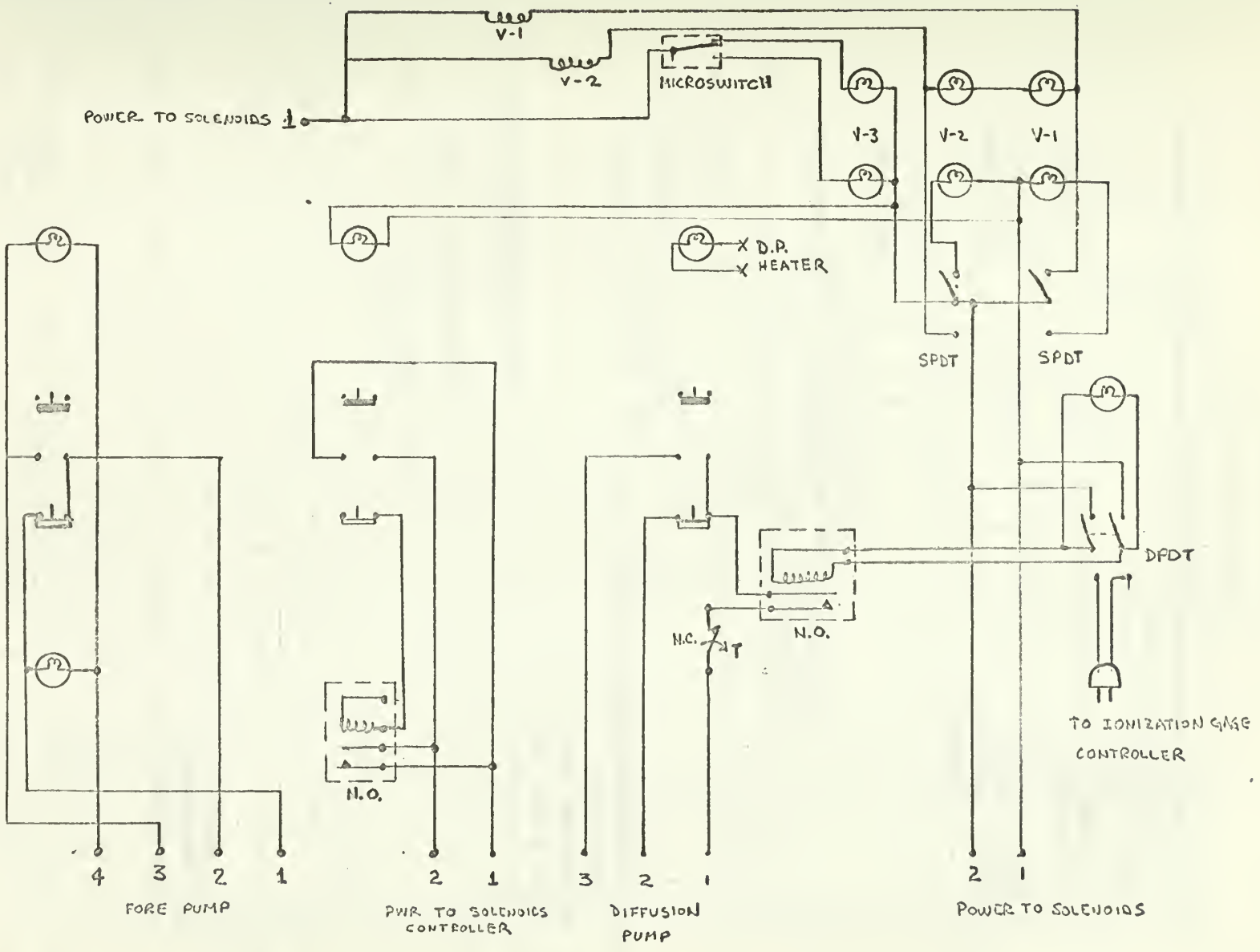

FIG. 15 CIRCUIT DIAGRAM OF CONTROLS

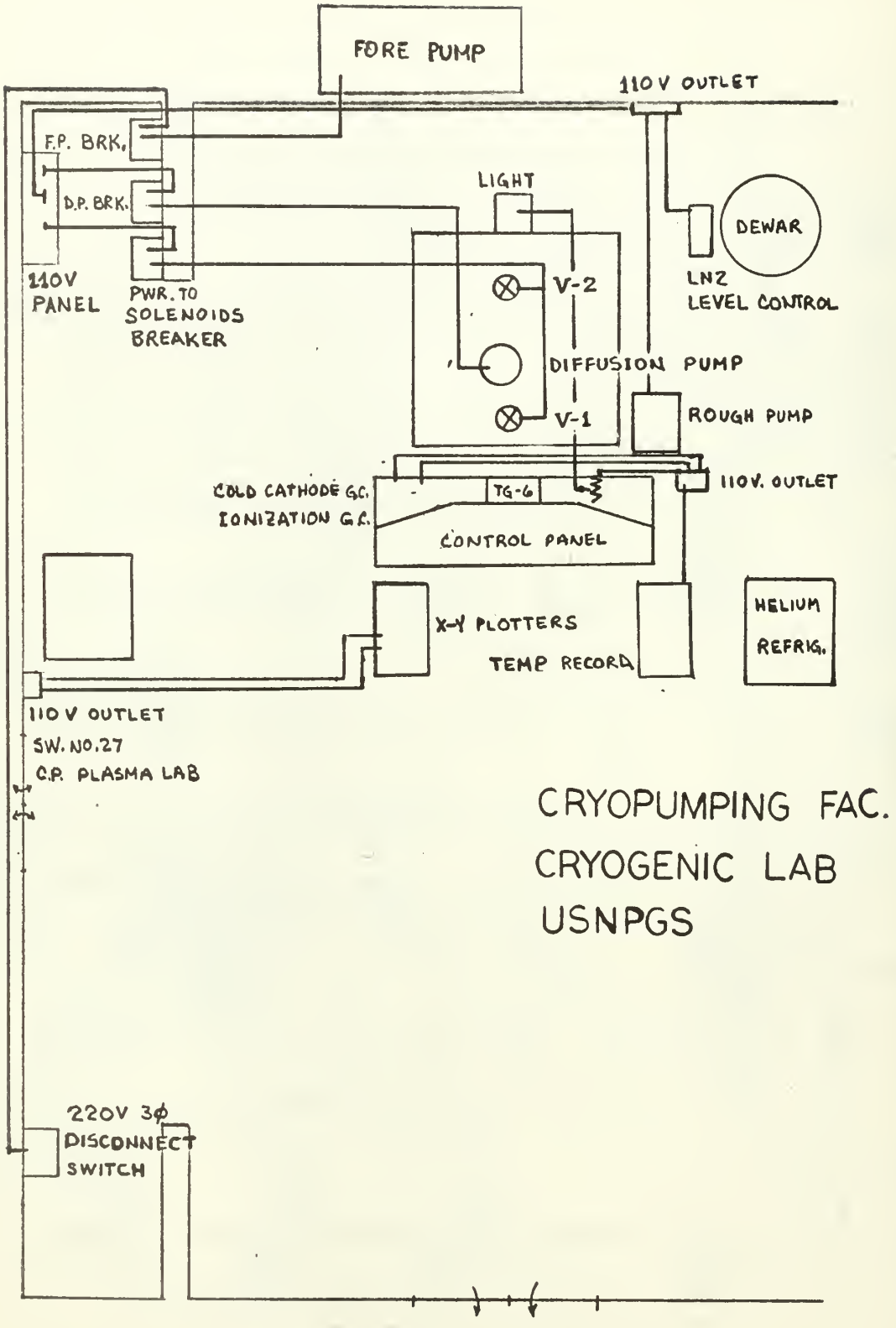

FIG. 16 ELECTRICAL LINE DIAGRAM

APPENDIX III

Gas Flow Measurement

A schematic diagram of the gas addition system employed is shown in Fig. 17. The principle of operation is to evacuate a known volume V_L and measure the rate of pressure rise in that volume, thereby giving an indication of flow in terms of torr-liters/sec. The flow will not be affected by upstream pressure if it is greater than the critical pressure ratio which ranges from about 0.5 for viscous flow to 0.05 for free molecular flow (21).

The known volume and piping to the gas bottle was first evacuated with the roughing pump to 30 μ and then with the high vacuum system to less than 1 μ . All valves were then closed and the pressure rise noted for background leakage.

The variable leak valve was then set to an approximate value indicated on the counter. The plotter for the thermocouple gage was started and the valve to the gas bottle opened. A sample of the pressure rise graph is given in Fig. 19. The volume was then roughed down prior to opening the valve to the high vacuum chamber.

To obtain pressure rise graphs by use of a thermocouple gage first requires calibration of the gage. The procedure employed was as recommended by the manufacturer in setting the filament current when the pressure is below 1 μ. The graph paper on an X-Y plotter was then calibrated for various pressures as indicated on the meter. The resulting record on non-linear coordinates was transformed to linear coordinates on the same graph. Note that the actual output in Fig. 19 and the linear plot also differ in pressures for the same time. A pressure correction was

necessary for CO_2 as the indicating meter for the thermocouple gage is calibrated for air or Nitrogen; the correction curve is shown in Fig. 18.

A pressure rise slope was then taken at about 300 μ which was an average value for P_L when gas was being injected into the chamber. Since the flow developed is in the transition region, the flow rate will vary with P_L and thus the slope should be taken at noted values of P_L.

The variation of Q_L with the pressure drop across the variable leak valve is due to the changing nature of the flow and the conductance effect to the thermocouple gage. In the free molecular flow regime the flow varies linearly with $(P_o - P_L)$ whereas in the visions region the flow is proportional to $(P_o^2 - P_L^2)$ (6).

Although the pressure drop is so great that the pressure downstream of the variable leak valve should not be affected, the flow to the thermocouple gage is subjected to changes from free molecular to viscous flow region.

A consideration in final computation of flow rate should be temperature effects of the expanding gas as it enters V_L with a reduction in pressure from 760 to .1 mm Hg.

One would expect a temperature drop from the sudden expansion with a corresponding effect on the thermocuple gage reading since it is temperature sensitive, however, a check on the flow rate by pressure rise in the chamber shows the isothermal condition to hold. Thus, although the exact nature of the flow is uncertain, it can be assumed that molecular collisions with the walls of V_e maintains the temperature of the gas at a nearly constant level. The pressure rise is sufficiently slow and flow rates so small that heat transfer with the walls is complete within a very short time.

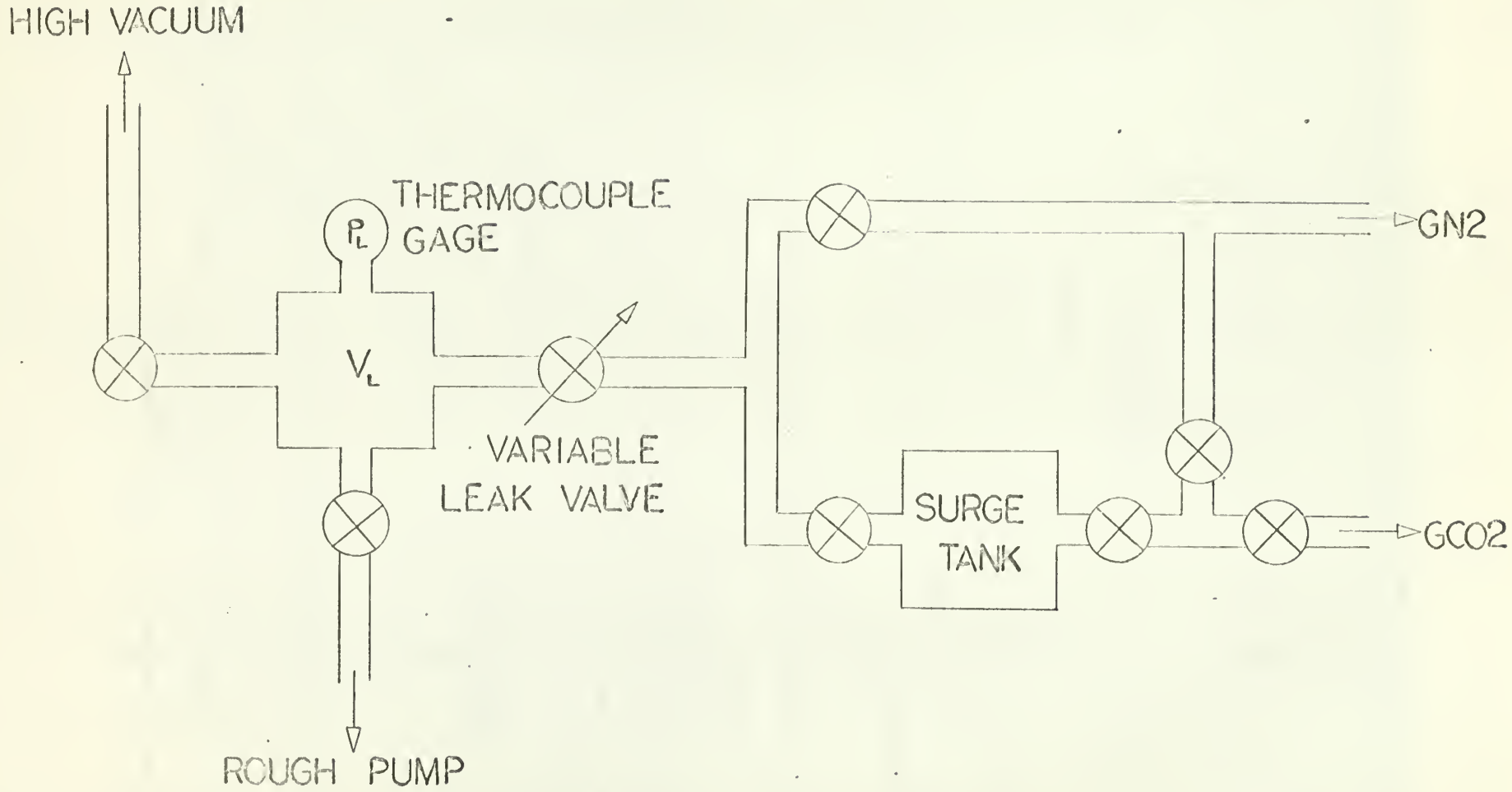

FIG. 17 SCHEMATIC OF GAS ADDITION SYSTEM

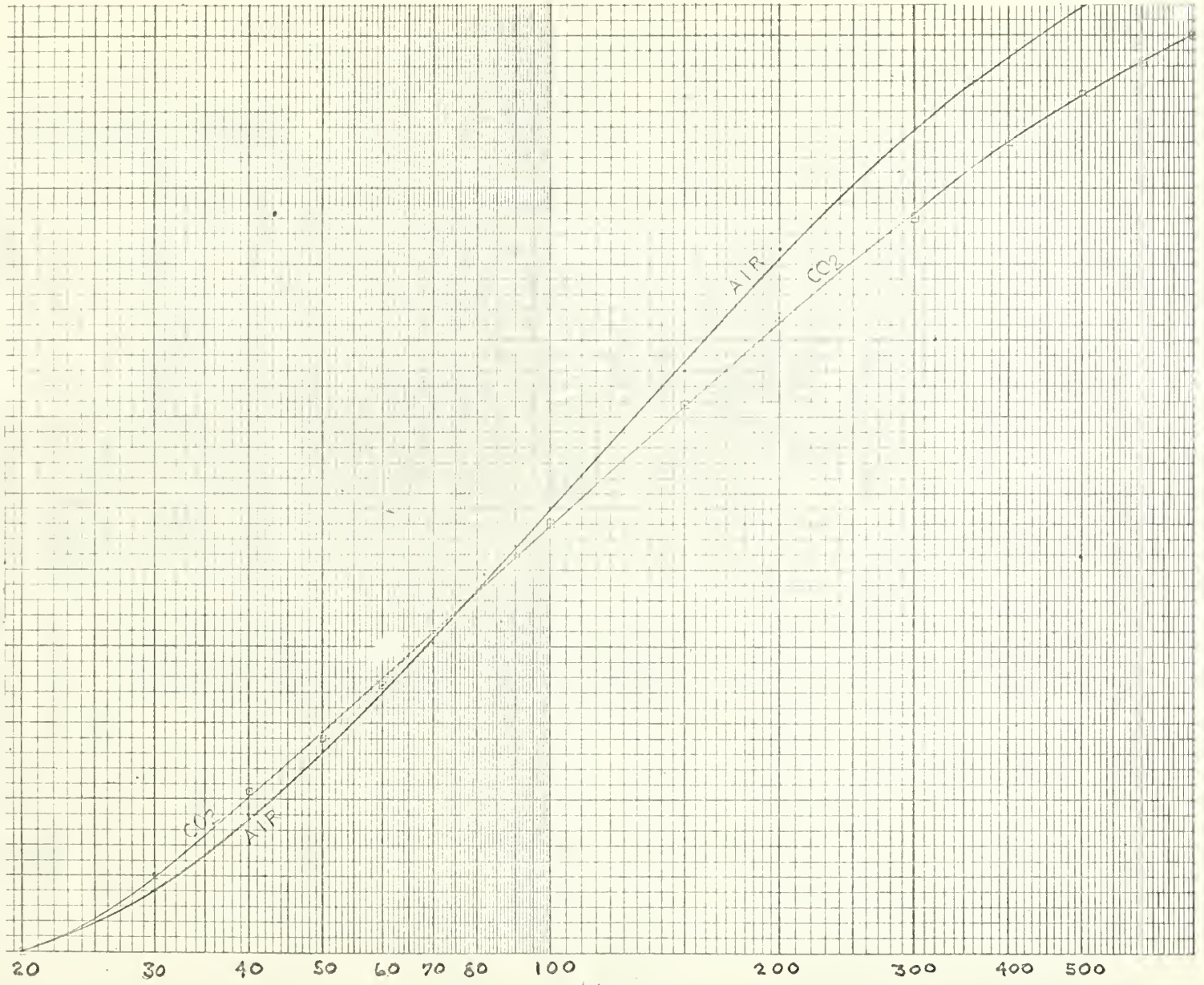

FIG. 18 THERMOCOUPLE GAGE PRESSURE CORRECTION

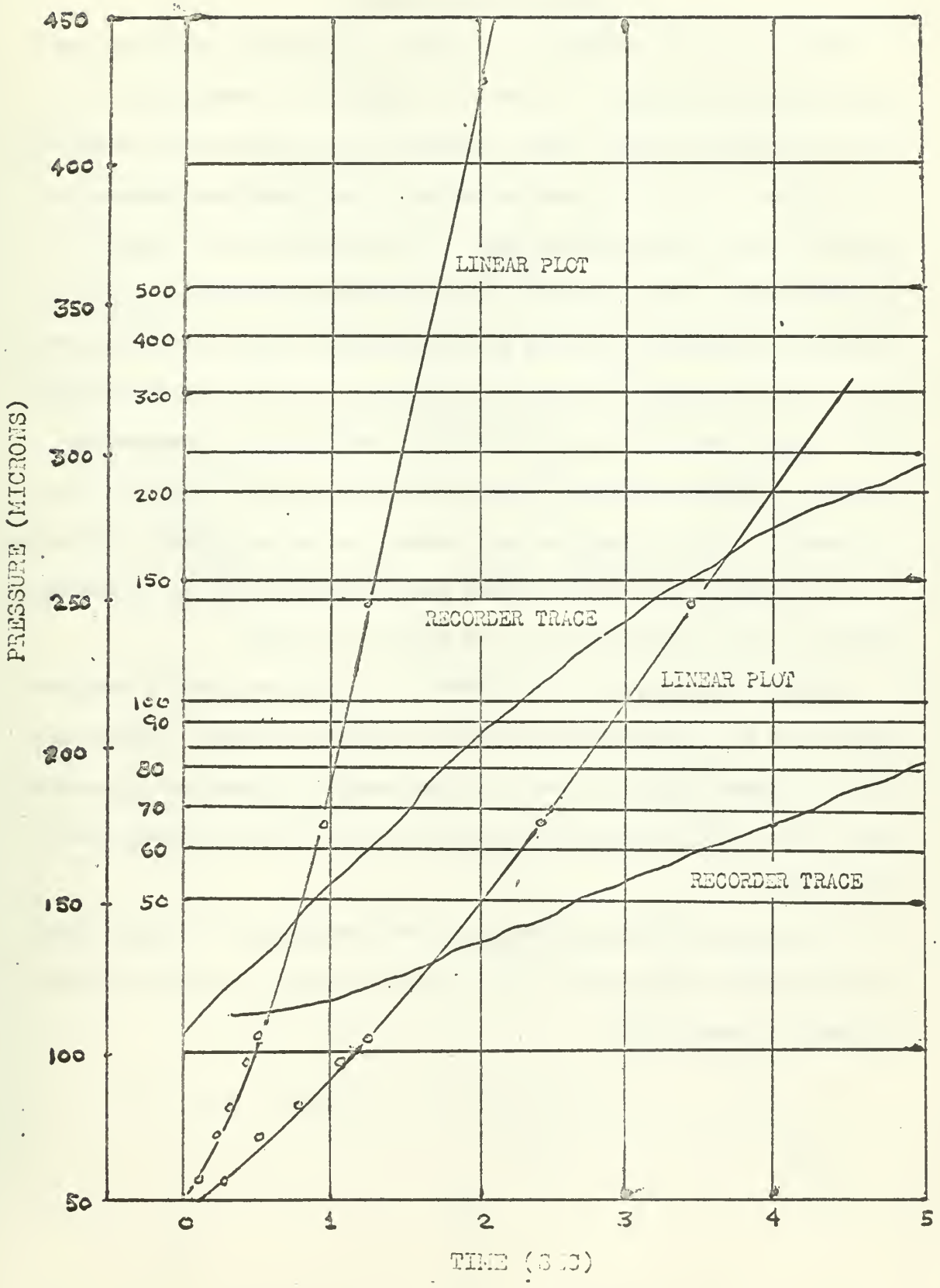

FIG. 19 SAMPLE FLOW MEASUREMENT

APPENDIX IV

Temperature Measurement

The importance of insuring uniformity of surface temperature has been discussed previously. In order to measure the temperatures, 19 teflon insulated 24 gauge copper constantan thermocouples were distributed as shown in Fig. 20. Each thermocouple was beaded and soldered to the metal wall at the junction with low temperature solder - used for stainless steel. The effect of stray currents and common loops well avoided by completely isolating each thermocouple except at the solder point. The reference junction was completely insulated and the coaxial cable feeding the signal to a differential amplifier was grounded to the tank to minimize induced voltage on the leads. The output of the differential amplifier was fed to a digital voltmeter-printer combination. On a slow scan, the printer recorded each temperature as the thermocouple selector switch was rotated to a new position by hand.

Sample thermocouples were soldered to a stainless steel tubing and immersed in LN_2, LOX, and ice to obtain reference voltages. These calibration voltages were then used in a NBS computer program which printed table values for temperatures and emfs for ice and LN_2 reference junctions (22).

Voltages from different junctions were reproduceable within 20 μV. for LN2-ICE and within 10 μV. for LDX-LN2, giving an accuracy of about $\frac{1}{2}$°K and 1°K respectively.

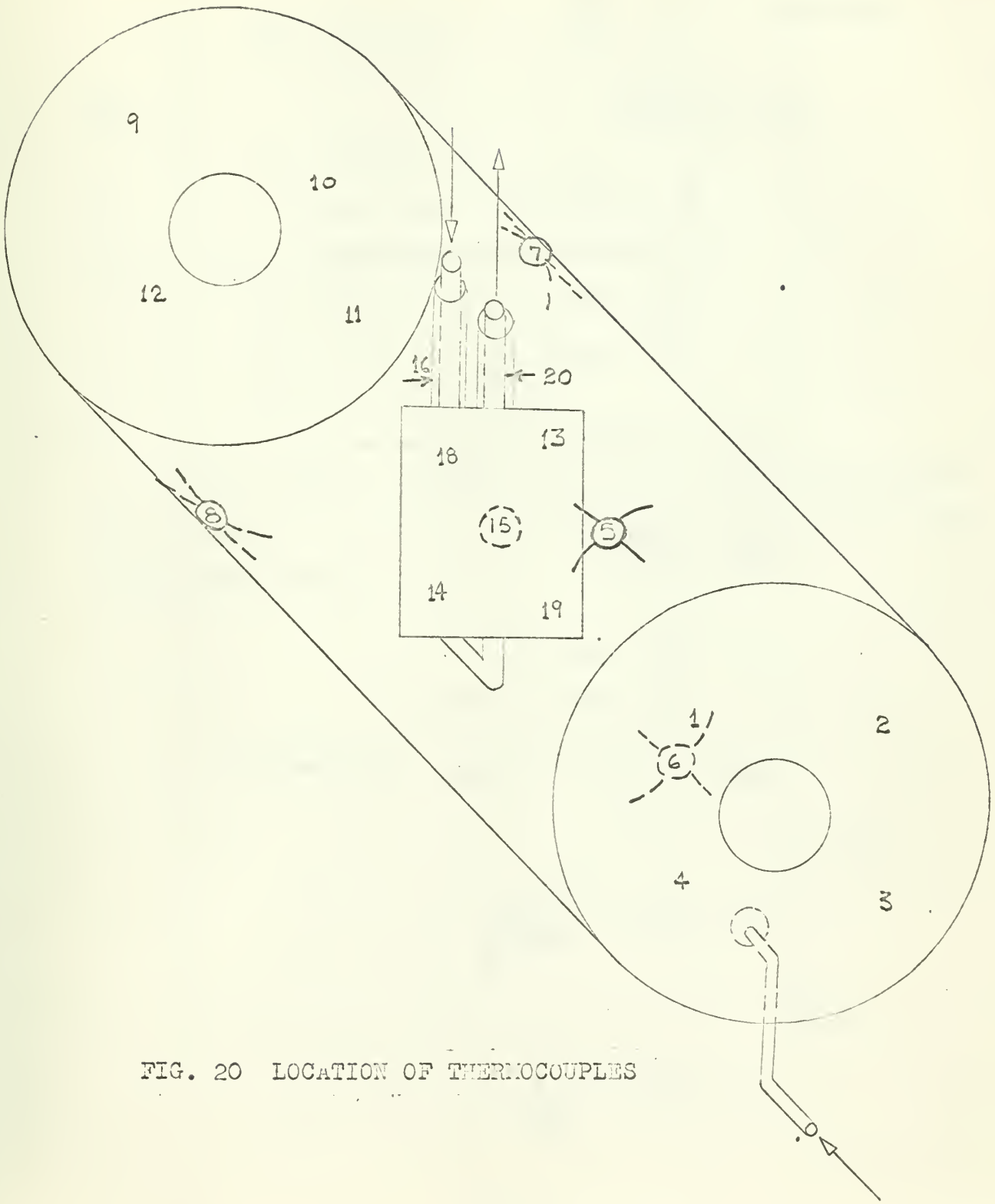

FIG. 20 LOCATION OF THERMOCOUPLES

APPENDIX V

Calculation of the Capture Coefficient

Definition $$C = \frac{S_{EXP}}{S_{th}}$$

$$S_{th} = \sqrt{\frac{R_M T_g}{2\pi M}}$$

$R_M = 8.315 \times 10^7$ erg/°K - gm-mole

$M = 44.0$ gm/gm-mole for CO_2

$T_g = [°K]$

$\pi = 3.142$

$$S_{th} = 0.548\, T_g^{1/2} \quad \text{liters/sec-cm}^2$$

$$S_{EXP} = \frac{\dot{P}_L V_L}{\Delta P A_P}$$

$V_L = 80 \pm 1$ cc

$A_P = 3120 \pm 300$ cm^2

$$S_{EXP} = 2.55 \times 10^{-5}\, \dot{P}_L / \Delta P \quad \text{liters/sec-cm}^2$$

for CO_2

$$C = 4.65 \times 10^{-5} \frac{\dot{P}_L}{\Delta P \sqrt{T_g}}$$

at 300°K

$$C = 2.69 \times 10^{-6} \frac{\dot{P}}{\Delta P}$$

since the ionization gage is calibrated for N_2

$$\Delta P_m = 1.37\,\Delta P$$

then

$$C = 3.69\times10^{-6}\,\frac{\dot{P}}{\Delta P_m}$$

if $\dot{P}$ is expressed in μ/sec

$$\boxed{C = 3.69\times10^{-9}\,\frac{\dot{P}_\mu}{\Delta P_m}}$$

The above equation is plotted in Fig. 21. The corresponding figure for N_2 is plotted in Figure 22. The above figures give results well within experimental error.

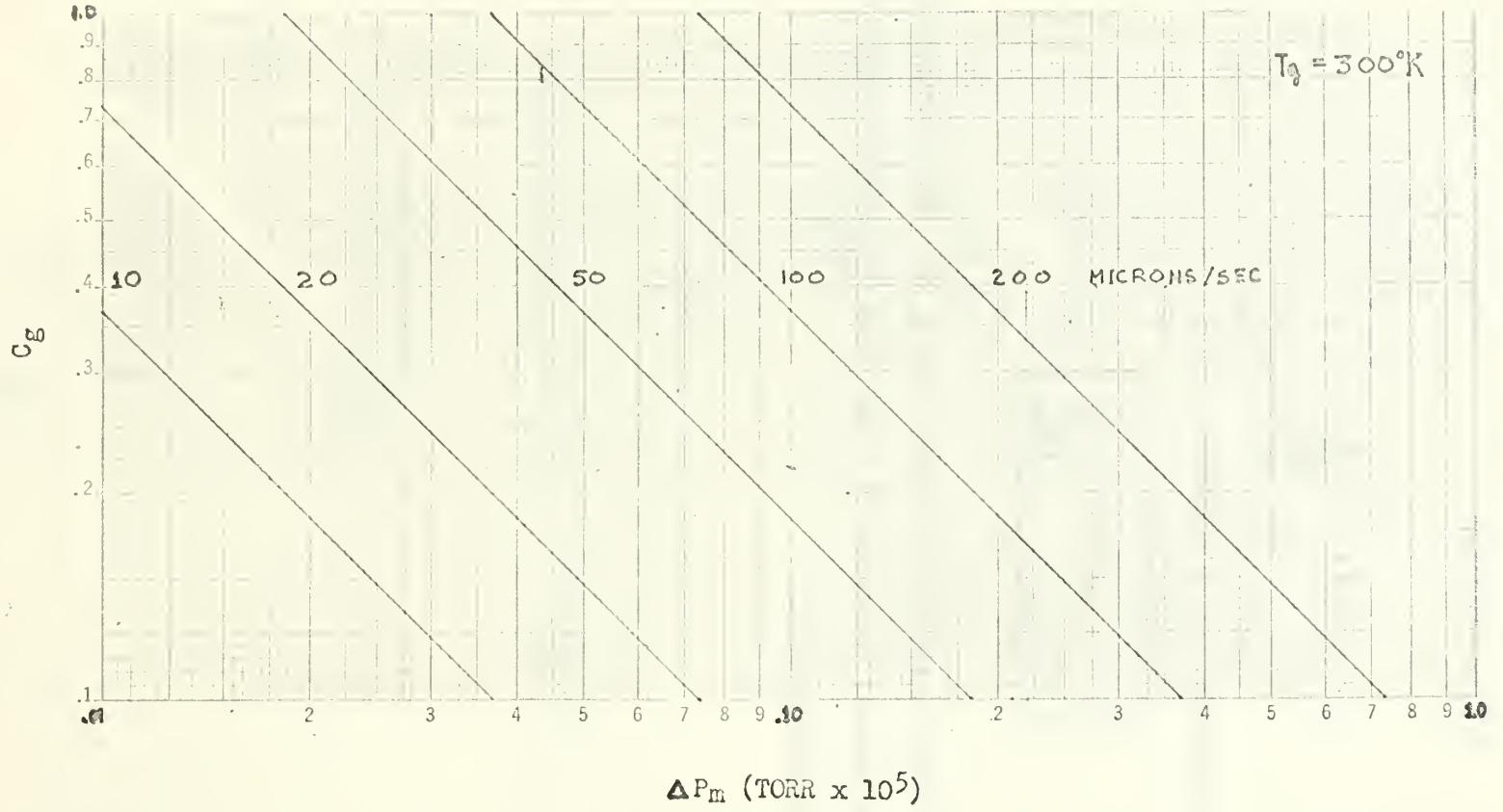

FIG. 21 CONDENSATION COEFFICIENTS OF 300°K CO_2

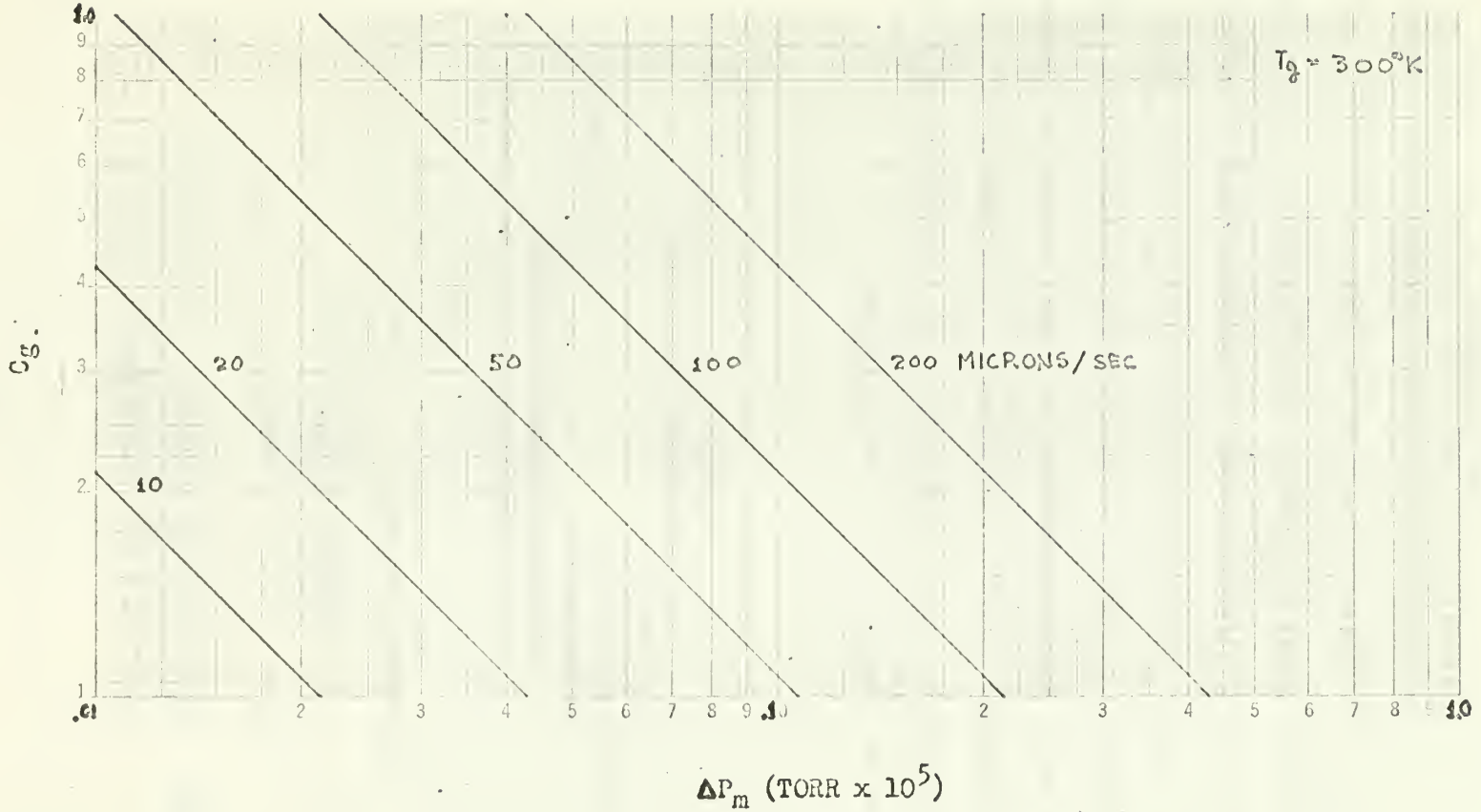

FIG. 22 CONDENSATION COEFFICIENTS OF 300°K N_2

APPENDIX VI

DESIGN AND CONSTRUCTION OF GASEOUS HELIUM TRANSFER LINES

The A.D. Little Helium Refrigerator available for this experiment has the refrigeration capacity described in Fig. 23. It was necessary to provide lines to transfer the cold helium to the cryopanel.

The design of transfer lines for cryogenic fluids is characterized by three factors. Insulation is essential and a vacuum jacket over the conducting line is the most efficient means of insulation. Linear contraction due to great temperature differentials must be considered, as well as flexibility of the line so as to reduce excessive stresses.

The resulting design shown in Fig. 25 allows ample flow of Helium to utilize the capacity of the refrigerator.

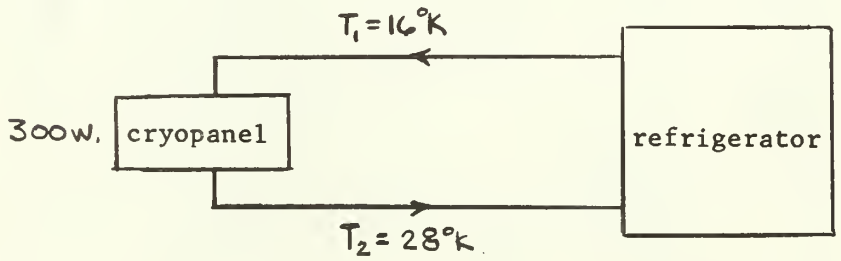

Properties of Helium

$16°K$ $1/\rho = 325.24$ cc/gm
$h_1 = 96.77$ joules/gm

$28°K$ $1/\rho = 574.13$ cc/gm
$h_2 = 159.67$ joules/gm

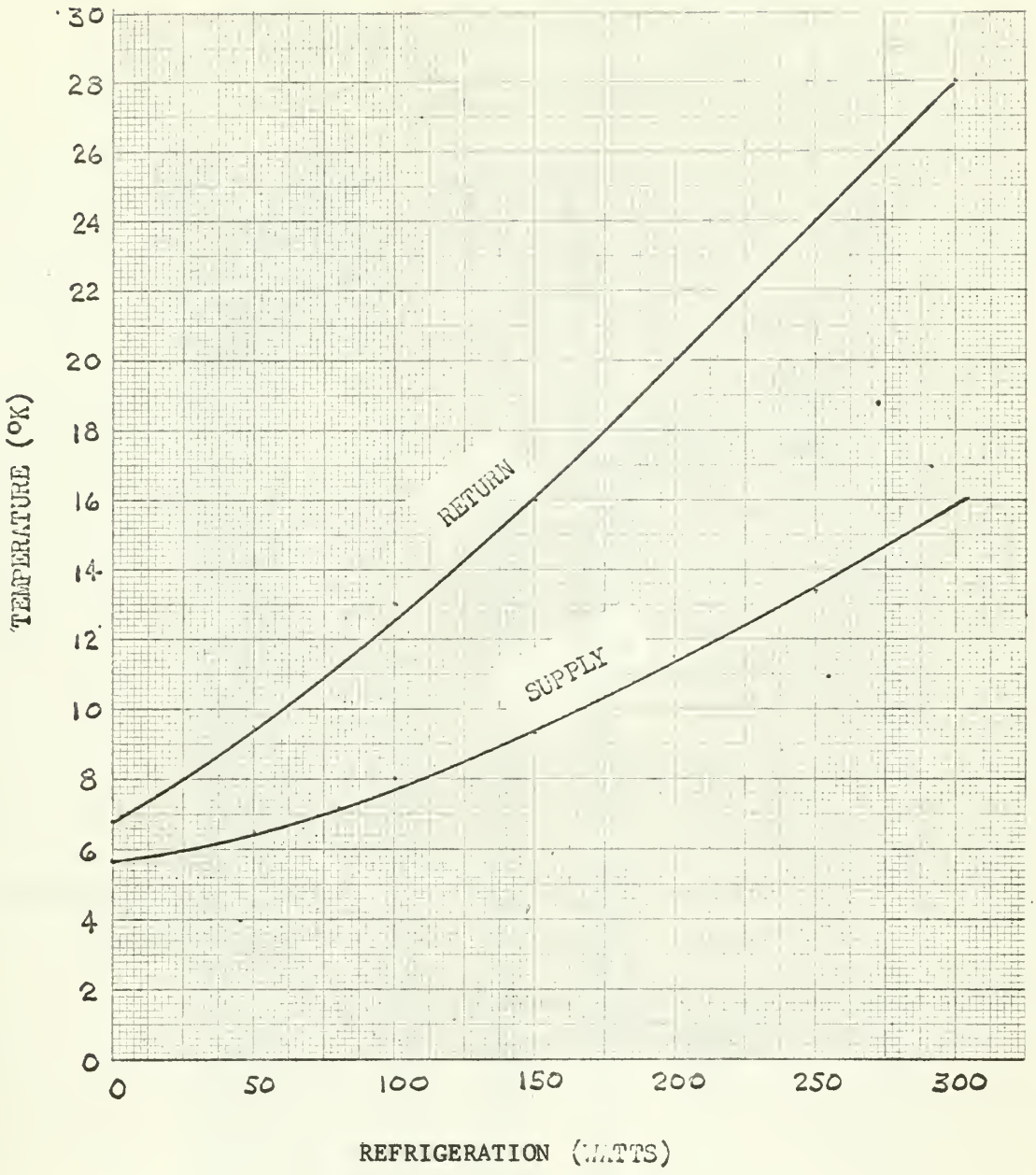

FIG. 23 HELIUM REFRIGERATOR LOADING

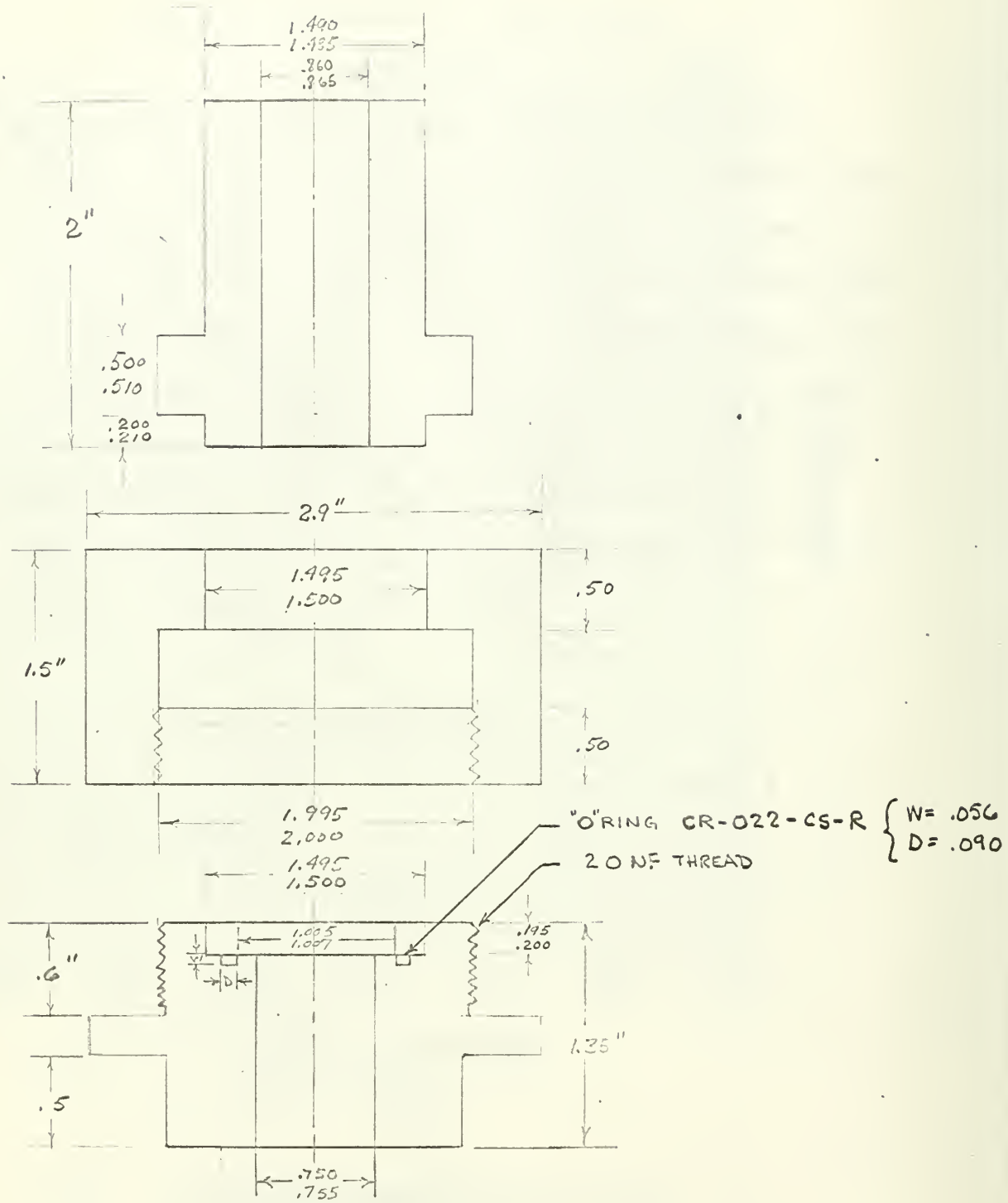

FIG. 24 HELIUM COUPLING

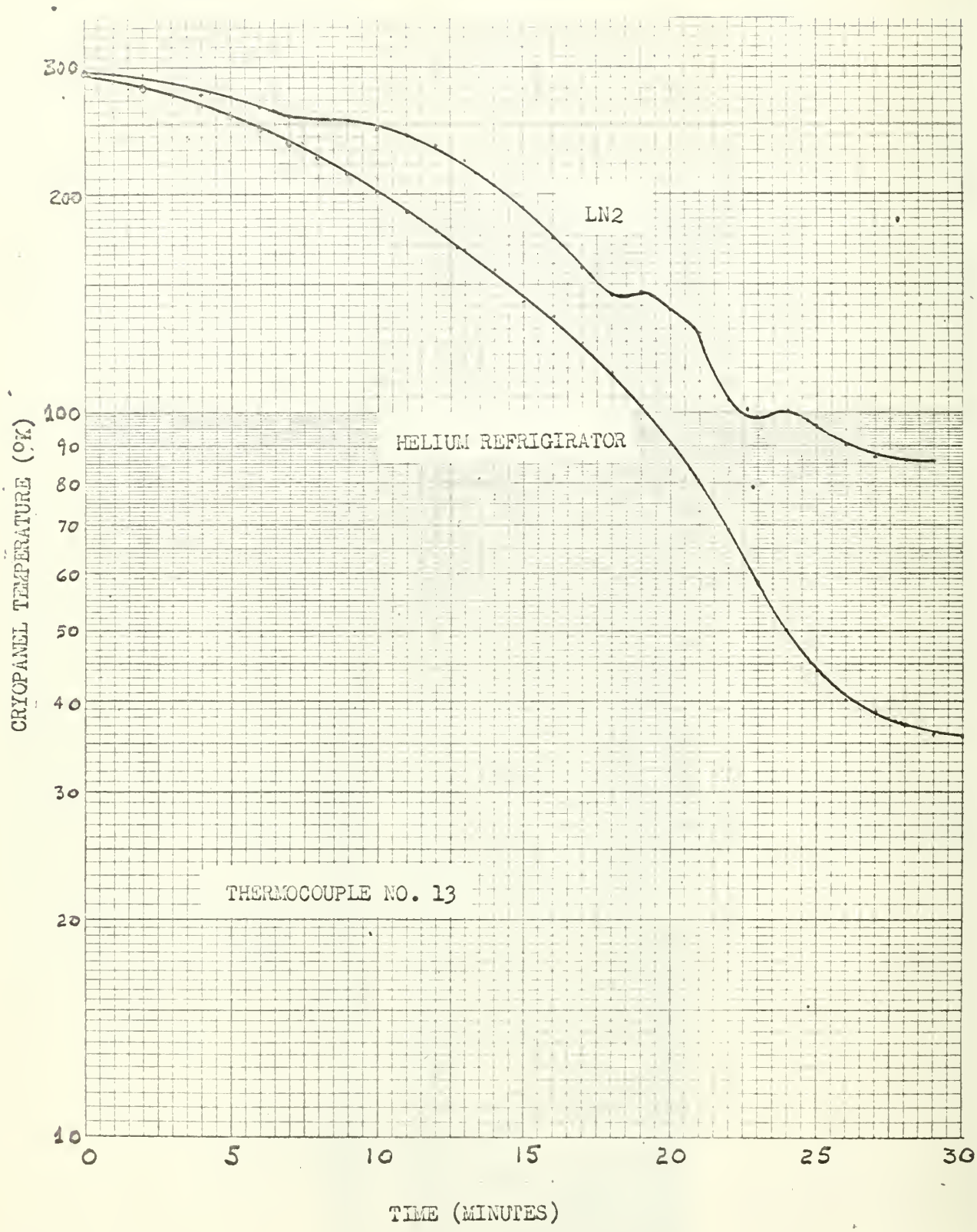

FIG. 26 COOLDOWN CURVES FOR CRYOPANEL.

$$Q = \dot{m}\,(h_2 - h_1)$$

$$\dot{m} = \frac{300 \text{ watts}}{(159.67 - 96.77)\ \text{joules/gm}}$$

$$\dot{m} = 4.77 \text{ gm/sec}$$

limit on flow rate would occur at higher temperature

$$d = .375 - .070 = .305 \text{ in}$$

$$d = 0.775 \text{ cm}$$

$$\mu = 45 \times 10^{-6} \text{ poise}$$

$$Re = \frac{4\dot{m}}{\pi d \mu}$$

$$Re = \frac{(4)(4.77 \text{ gm/sec})}{(3.142)(.775 \text{ cm})(45 \times 10^{-6} \text{ gm/sec-cm})}$$

$$\boxed{Re = 1.74 \times 10^5}$$

$$V = \frac{4\dot{m}}{\pi \rho d^2}$$

$$V = \frac{(4)(4.77 \text{ gm/sec})}{(3.142)\left(\frac{1}{574.13 \text{ gm/cc}}\right)(.775 \text{ cm})^2}$$

$$V = 5800 \text{ cm/sec}$$

$$\boxed{V = 58 \text{ m/sec}}$$

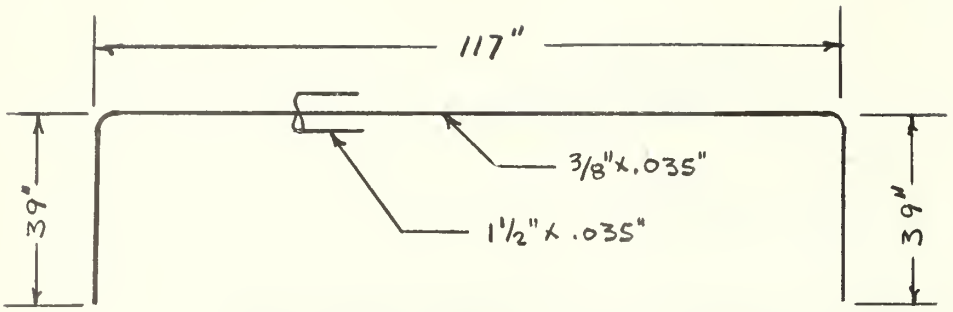

lines cooled from 300°K. From Scott (15) for 304 Stainless Steel

$$20°K \quad \Delta L/L_o = -1.1 \times 10^{-5}$$

$$300°K \quad \Delta L/L_o = 304 \times 10^{-5}$$

$$\Delta L/L_o = 305 \times 10^{-5}$$

total shrinkage $\Delta L = (3.05 \times 10^{-3})(.195 \times 10^{3}\ IN) = 0.595\ IN$

span $\Delta L = (3.05 \times 10^{-3})(.117 \times 10^{3}\ IN) = 0.357\ IN$

heighth $\Delta L = (3.05 \times 10^{-3})(.039) \times 10^{3}\ IN) = 0.119\ IN$

The total shrinkage is within the tolerances allowed by the outer jacket

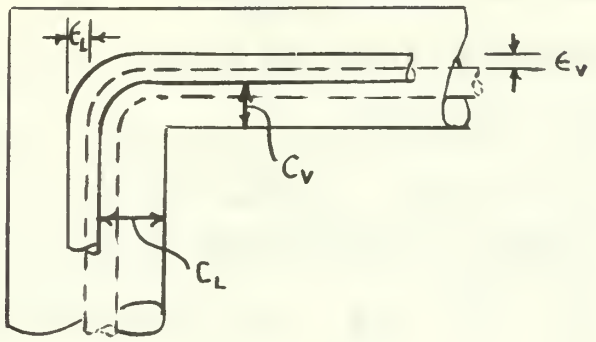

$$\epsilon_L = \frac{0.357}{2} = 0.179 \text{ in}$$

$$\epsilon_v = 0.119$$

$$2\,C_L = (1.500 - .070) - 0.375 = 1.055$$

$$C_L = 0.527$$

$$C_V = C_L$$

$$C_L - \epsilon_L = 0.527 - 0.179 = 0.348 \text{ inches}$$

$$C_v - \epsilon_v = 0.527 - 0.119 = 0.408 \text{ inches}$$

The inner tube was maintained in position by triangular 0.020" stainless steel retainers. The conductance of these retainers is negligible since contact to the outer jacket is through three points, the conductivity of stainless steel is very low, and the retainer is very thin.

Heat loss in transfer lines can be calculated

Conduction

Knudsen's equation for heat transfer between long coaxial cylinders

$$W = 2.426 \times 10^{-4} A_1 \frac{\alpha_1 \alpha_2}{\alpha_2 + \frac{A_1}{A_2}(1-\alpha_2)\alpha_1} \frac{\gamma+1}{\gamma-1} \frac{P}{\sqrt{MT}} (T_2 - T_1)$$

W = [watts]

A_1, A_2 = area inner & outer walls [cm^2]

P = pressure [in microns Hg] = 1μ

$T_1 = 20°K \quad T_2 = 300°K$

$\alpha_1 = 0.9 \quad \alpha_2 = 1.0$ Scott ref (15)

γ = 1.4 ratio of specific heats for air

$\frac{A_1}{A_2} = \frac{d_1}{d_2} = \frac{.375}{1.5} = .25 \qquad A_1 = \frac{\pi}{4}(.375)^2(515) = 32.6\ cm^2$

Radiation

Consider two coaxial long cylinders under going radiation energy exchange by diffuse reflection

$$W = \sigma E A_1 (T_2^4 - T_1^4) \qquad \sigma = 5.67 \times 10^{-12}\ watt/cm^2 \cdot °K$$

where

$$E = \frac{e_1 e_2}{e_2 + \frac{A_1}{A_2}(1-e_2)e_1}$$

The emmissities are given for unpolished SS

20°K $\quad e_1 = .2$

300°K $\quad e_2 = .4$

$E = .186$

$W_{RAD} = .279$ WATTS

The total heat loss for each transfer tube is then

$W_T = W_{COND} + W_{RAD}$

$W_T = .169 + .279$

$W_T = .448$ WATTS

APPENDIX VII

Plant Simulation

The equations for the plant dynamics derived in Section 4 were solved by Analog computer techniques. The equations and corresponding analog equations follow where the bar distinguishes voltages from actual values and includes scale factors as well as coefficients

$$\dot{P}_c = \pi + a_1 P_1 + a_2 P_e - A P_c \tag{4.32}$$

$$\bar{P}_c = -\int (w_1 \bar{\pi} + w_2 \bar{P}_1 + w_3 \bar{P}_e - w_4 \bar{P}_c)\, dt \tag{VII-1}$$

$$\dot{P}_1 = \pi_3 + a_6 P_c - (a_7 + a_8) P_1 \tag{4.33}$$

$$\bar{P}_1 = -\int (w_5 \bar{\pi}_3 + w_6 \bar{P}_c - w_7 \bar{P}_1)\, dt \tag{VII-2}$$

$$\dot{P}_e = \pi_4 + a_9 \bar{P}_c - a_{10} \bar{P}_e \tag{4.34}$$

$$\bar{P}_e = -\int (w_8 \bar{\pi}_4 + w_9 \bar{P}_c - w_{10} \bar{P}_e)\, dt \tag{VII-3}$$

Considering the effect of value closing time

$$\bar{Q}_L - \bar{Q}_{L0} = -\int \left(\frac{w_{11}}{t_c}\right) dt \tag{VII-4}$$

where Q_{L0} = initial flow rate

t_c = value closing time

each w factor represents values of electrical components

$$w_i = \frac{b}{R_{in} C_f} \tag{VII-5}$$

for an intergrator, and for a summer

$$w_i = \frac{b R_f}{R_{in}} \tag{VII-6}$$

where

b = potentiometer setting

R_{in} = input resistor

R_f = feedback resistor

C_f = feedback capacitor

The values of components and resulting values of the coefficients are tabulated in Table V. The complete diagram of the system is shown in Fig. 27.

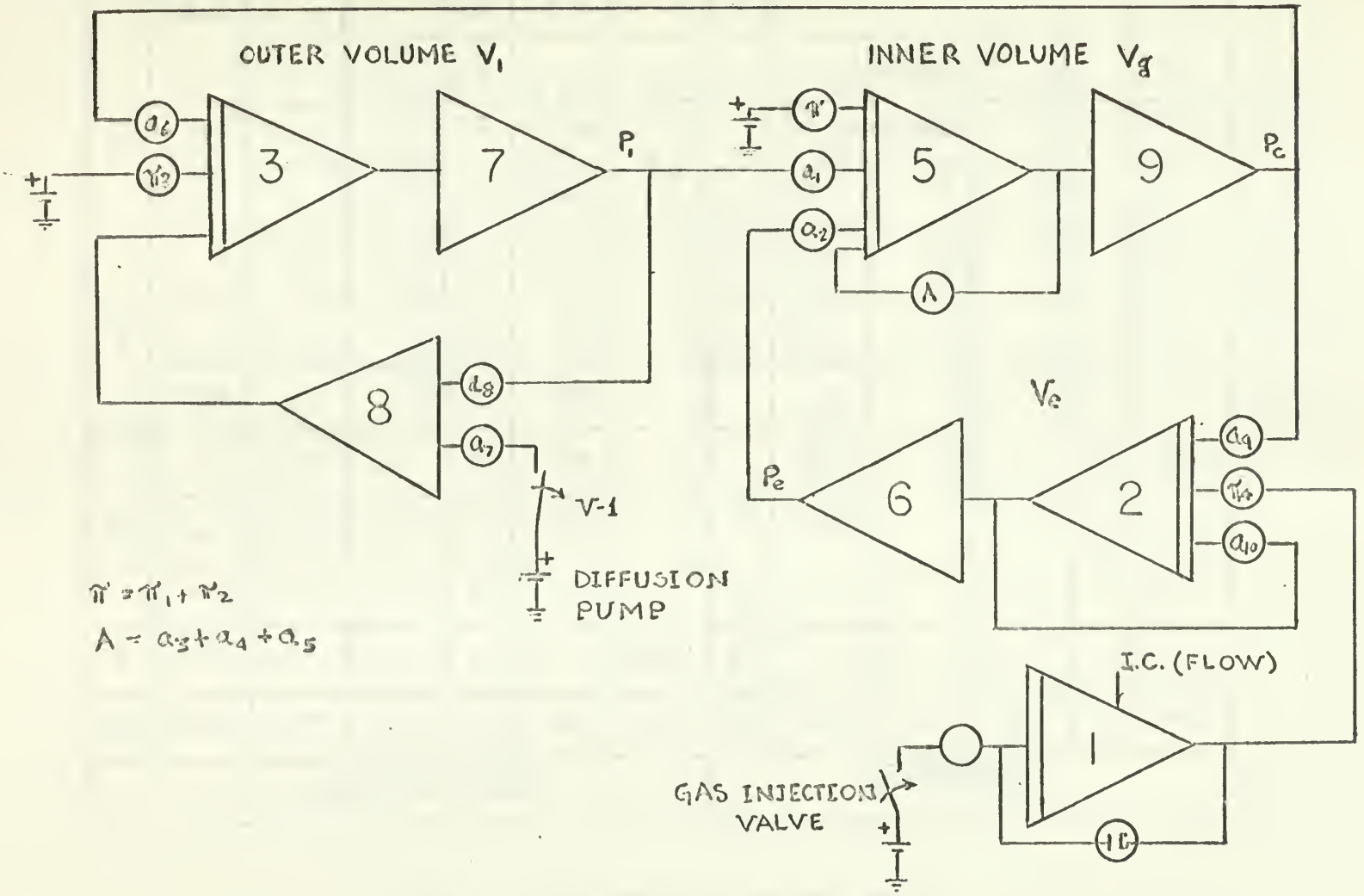

FIG. 27 ANALOG SIMULATION OF SYSTEM

TABLE V ANALOG COMPUTER COMPONENT VALUES

INTEGRATOR							SUMMER					
NO.	POT	R_{IN}	C_f	i	w_i	I.C.	NO.	POT	R_{IN}	R_f	i	w_i
1	.540	1	1	11	.540	48v.	6	—	1	1	—	1
2	—	1	1	8	1		7	—	1	1	—	1
	—	1	1	10	1		8	.280	1	.1	$(7)_1$	.280
	—	10	1	9	.100			—	1	1	$(7)_2$	1.000
3	.200	1	1	5	.200							
	—	1	1	6	1							
	—	—	1	7	1							
5	.192	1	1	1	.192							
	.626	1	1	2	.1626			R (MEGAOHMS)				
	—	1	1	3	1			C (MICROFARADS)				
	.415	.1	1	4	4.15							

INITIAL DISTRIBUTION LIST

		No. Copies
1.	Defense Documentation Center Cameron Station Alexandria, Virginia 22314	20
2.	Library U. S. Naval Postgraduate School Monterey, California	2
3.	Naval Ship Systems Command Navy Department Washington, D. C. 20360	1
4.	Mechanical Engineering Department U. S. Naval Postgraduate School Monterey, California	1
5.	Prof. P. F. Pucci Mechanical Engineering Department U. S. Naval Postgraduate School Monterey, California	5
6.	LT L. C. Tedeschi, USN Supervisor of Shipbuilding, U.S. Navy Bath Iron Works Bath, Maine	2
7.	LCDR Carl Albero, USN Supervisor of Ship Building, U. S. Navy Bath Iron Works Bath, Maine	1
8.	LCDR George M. LaChance Naval Ship Systems Command Code 1500 Navy Department Washington, D. C. 20360	1

Unclassified
Security Classification

DOCUMENT CONTROL DATA - R&D

(Security classification of title, body of abstract and indexing annotation must be entered when the overall report is classified)

1. ORIGINATING ACTIVITY (Corporate author)	2a. REPORT SECURITY CLASSIFICATION
U. S. Naval Postgraduate School Monterey, California	Unclassified
	2b. GROUP N.A.

3. REPORT TITLE

Capture Coefficients of Carbon Dioxide and Nitrogen Gas on a Cryogenic Cooled Surface

4. DESCRIPTIVE NOTES (Type of report and inclusive dates)

N.A.

5. AUTHOR(S) (Last name, first name, initial)

TEDESCHI, Louis Carmelo, LT, USN

6. REPORT DATE	7a. TOTAL NO. OF PAGES	7b. NO. OF REFS
May 1966	89	22

8a. CONTRACT OR GRANT NO.	9a. ORIGINATOR'S REPORT NUMBER(S)
N.A.	N.A.
b. PROJECT NO. N.A.	
c.	9b. OTHER REPORT NO(S) (Any other numbers that may be assigned this report) N.A.
d.	

10. AVAILABILITY/LIMITATION NOTICES

This document has been approved for public release and sale; its distribution is unlimited.

~~Qualified requesters may obtain copies of this report from DDC~~ Mer 9/23/71

11. SUPPLEMENTARY NOTES	12. SPONSORING MILITARY ACTIVITY
N.A.	U. S. Navy

13. ABSTRACT

Capture coefficients of CO_2 and N_2 were measured on a flat cryopanel. The cryopumping of 300°K CO_2 on an 85°K surface resulted in a capture coefficient of 0.58 while for 300°K N_2 on a 33°K surface a coefficient of 0.65 was measured.

The pressure drop method employed to measure the above capture coefficients was studied to account for vapor pressure, temperature corrections, and assumptions which must be made in the calculation of the capture coefficient. An analog model of the actual system was capable of predicting system pressure responses.

Instrumentation and construction of gaseous helium transfer lines necessary to effect the above measurements are also discussed.

DD FORM 1 JAN 64 1473

Unclassified
Security Classification

14. KEY WORDS	LINK A		LINK B		LINK C	
	ROLE	WT	ROLE	WT	ROLE	WT
Cryopumping						
Capture Coefficients						
Helium refrigerator						
Cryogenic fluid transfer tubes						
High Vacuum						
Space simulation						
Molecular flow simulation						

INSTRUCTIONS

1. ORIGINATING ACTIVITY: Enter the name and address of the contractor, subcontractor, grantee, Department of Defense activity or other organization *(corporate author)* issuing the report.

2a. REPORT SECURITY CLASSIFICATION: Enter the overall security classification of the report. Indicate whether "Restricted Data" is included. Marking is to be in accordance with appropriate security regulations.

2b. GROUP: Automatic downgrading is specified in DoD Directive 5200.10 and Armed Forces Industrial Manual. Enter the group number. Also, when applicable, show that optional markings have been used for Group 3 and Group 4 as authorized.

3. REPORT TITLE: Enter the complete report title in all capital letters. Titles in all cases should be unclassified. If a meaningful title cannot be selected without classification, show title classification in all capitals in parenthesis immediately following the title.

4. DESCRIPTIVE NOTES: If appropriate, enter the type of report, e.g., interim, progress, summary, annual, or final. Give the inclusive dates when a specific reporting period is covered.

5. AUTHOR(S): Enter the name(s) of author(s) as shown on or in the report. Enter last name, first name, middle initial. If military, show rank and branch of service. The name of the principal author is an absolute minimum requirement.

6. REPORT DATE: Enter the date of the report as day, month, year; or month, year. If more than one date appears on the report, use date of publication.

7a. TOTAL NUMBER OF PAGES: The total page count should follow normal pagination procedures, i.e., enter the number of pages containing information.

7b. NUMBER OF REFERENCES: Enter the total number of references cited in the report.

8a. CONTRACT OR GRANT NUMBER: If appropriate, enter the applicable number of the contract or grant under which the report was written.

8b, 8c, & 8d. PROJECT NUMBER: Enter the appropriate military department identification, such as project number, subproject number, system numbers, task number, etc.

9a. ORIGINATOR'S REPORT NUMBER(S): Enter the official report number by which the document will be identified and controlled by the originating activity. This number must be unique to this report.

9b. OTHER REPORT NUMBER(S): If the report has been assigned any other report numbers *(either by the originator or by the sponsor)*, also enter this number(s).

10. AVAILABILITY/LIMITATION NOTICES: Enter any limitations on further dissemination of the report, other than those imposed by security classification, using standard statements such as:

(1) "Qualified requesters may obtain copies of this report from DDC."

(2) "Foreign announcement and dissemination of this report by DDC is not authorized."

(3) "U. S. Government agencies may obtain copies of this report directly from DDC. Other qualified DDC users shall request through _____."

(4) "U. S. military agencies may obtain copies of this report directly from DDC. Other qualified users shall request through _____."

(5) "All distribution of this report is controlled. Qualified DDC users shall request through _____."

If the report has been furnished to the Office of Technical Services, Department of Commerce, for sale to the public, indicate this fact and enter the price, if known.

11. SUPPLEMENTARY NOTES: Use for additional explanatory notes.

12. SPONSORING MILITARY ACTIVITY: Enter the name of the departmental project office or laboratory sponsoring *(paying for)* the research and development. Include address.

13. ABSTRACT: Enter an abstract giving a brief and factual summary of the document indicative of the report, even though it may also appear elsewhere in the body of the technical report. If additional space is required, a continuation sheet shall be attached.

It is highly desirable that the abstract of classified reports be unclassified. Each paragraph of the abstract shall end with an indication of the military security classification of the information in the paragraph, represented as *(TS), (S), (C), or (U)*.

There is no limitation on the length of the abstract. However, the suggested length is from 150 to 225 words.

14. KEY WORDS: Key words are technically meaningful terms or short phrases that characterize a report and may be used as index entries for cataloging the report. Key words must be selected so that no security classification is required. Identifiers, such as equipment model designation, trade name, military project code name, geographic location, may be used as key words but will be followed by an indication of technical context. The assignment of links, roles, and weights is optional.

DD FORM 1 JAN 64 1473 (BACK)